Science Advances
AAAS

Supplementary Materials for

Cell size is a determinant of stem cell potential during aging

Jette Lengefeld*, Chia-Wei Cheng, Pema Maretich, Marguerite Blair, Hannah Hagen, Melanie R. McReynolds, Emily Sullivan, Kyra Majors, Christina Roberts, Joon Ho Kang, Joachim D. Steiner, Teemu P. Miettinen, Scott R. Manalis, Adam Antebi, Sean J. Morrison, Jacqueline A. Lees, Laurie A. Boyer, Ömer H. Yilmaz, Angelika Amon

*Corresponding author. Email: jette.lengefeld@helsinki.fi

Published 12 November 2021, *Sci. Adv.* **7**, eabk0271 (2021)
DOI: 10.1126/sciadv.abk0271

The PDF file includes:

Other Supplementary Material for this manuscript includes the following:

Figure S1

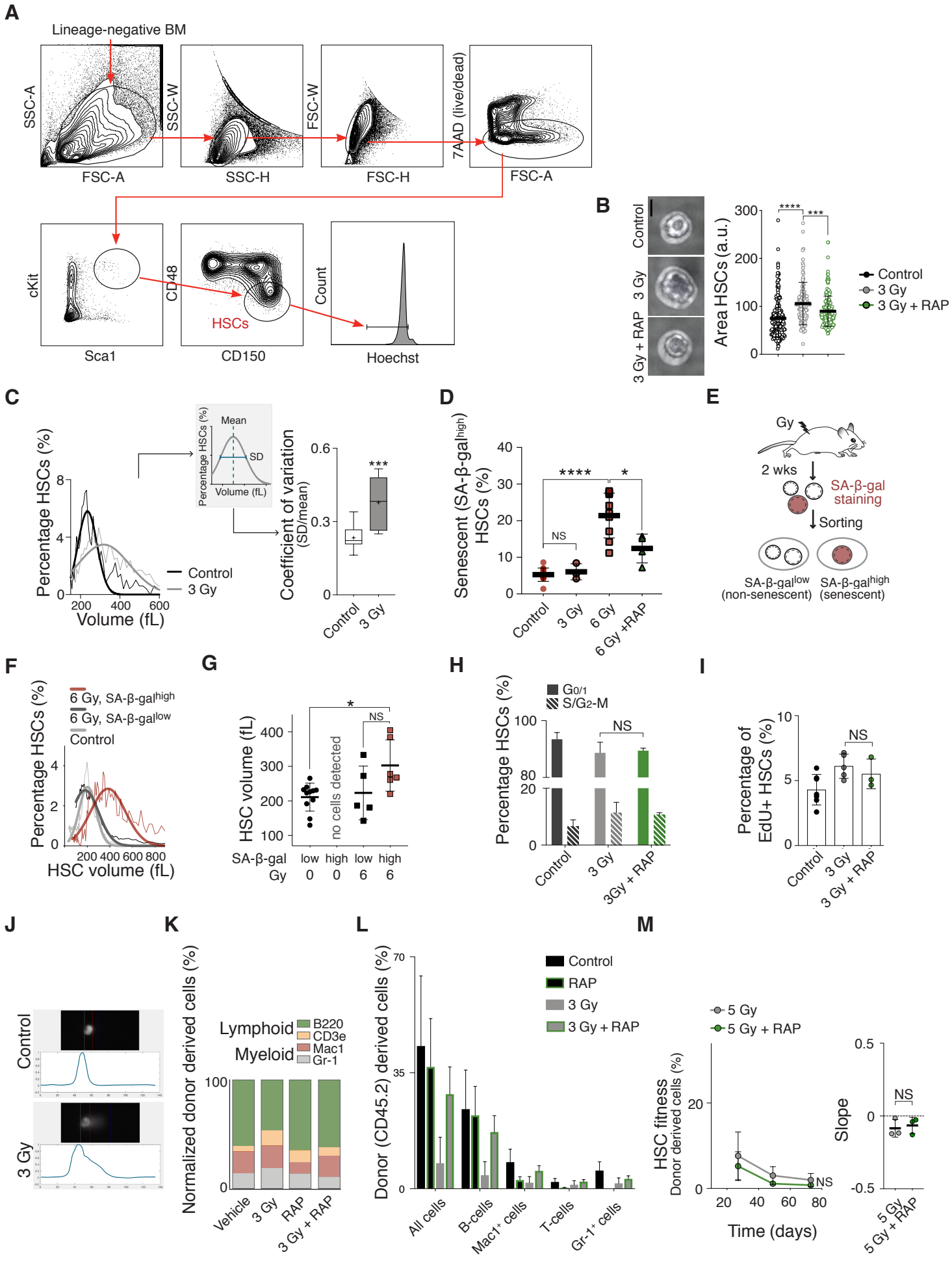
A
Lineage-negative BM
SSC-A
FSC-A
SSC-W
SSC-H
FSC-W
FSC-H
7AAD (live/dead)
FSC-A
cKit
Sca1
CD48
CD150
HSCs
Count
Hoechst
B
Control
3 Gy
3 Gy + RAP
Area HSCs (a.u.)
****
***
Control
3 Gy
3 Gy + RAP
C
Percentage HSCs (%)
Volume (fL)
Control
3 Gy
Mean
SD
Coefficient of variation (SD/mean)
***
D
Senescent (SA-β-gal^high) HSCs (%)
****
*
NS
Control
3 Gy
6 Gy
6 Gy +RAP
E
Gy
2 wks
SA-β-gal staining
Sorting
SA-β-gal^low (non-senescent)
SA-β-gal^high (senescent)
F
6 Gy, SA-β-gal^high
6 Gy, SA-β-gal^low
Control
Percentage HSCs (%)
HSC volume (fL)
G
HSC volume (fL)
*
NS
no cells detected
SA-β-gal
Gy
low high low high
0 0 6 6
H
G0/1
S/G2-M
Percentage HSCs (%)
NS
Control
3 Gy
3Gy + RAP
I
Percentage of EdU+ HSCs (%)
NS
Control
3 Gy
3 Gy + RAP
J
Control
3 Gy
K
Normalized donor derived cells (%)
Lymphoid
B220
CD3e
Myeloid
Mac1
Gr-1
Vehicle
3 Gy
RAP
3 Gy + RAP
L
Donor (CD45.2) derived cells (%)
Control
RAP
3 Gy
3 Gy + RAP
All cells
B-cells
Mac1+ cells
T-cells
Gr-1+ cells
M
5 Gy
5 Gy + RAP
HSC fitness
Donor derived cells (%)
NS
Time (days)
Slope
NS
5 Gy
5 Gy + RAP

Fig. S1: Enlargement of HSCs contributes to irradiation induced fitness decline

(**A**) Sorting protocol used to isolate BM-derived live $G_{0/1}$ (Hoechst) HSCs (Lin-, Sca1/Ly6+, CD117/cKit+, CD150/Slamf1+, CD48/Slamf2-, 7ADD-) from an 8-12 week-old mouse in representative FACS plots.
(**B**) Representative images of HSCs from control, sub-lethally irradiated (3 Gy) or 3 Gy + rapamycin (3 Gy + RAP) mice and quantification of HSC area (a.u., n > 150 HSCs per condition analyzed, scale bar is 5 μm).
(**C**) Representative raw data showing size distribution: Percentage of HSCs (%) per volume (fL) from control or 3 Gy irradiated mice 2 weeks after treatment. Scheme of standard deviation (SD) and mean of Gaussian distribution fitted to the size distribution of HSCs to calculate coefficient of variation (CV). CV (SD/mean) of control HSCs (n = 15) or DNA-damaged HSCs (3 or 6 Gy, n = 6).
(**D**) Percentage of senescent (SA-β-gal^{high}) HSCs (%) from control (n = 12), 3 Gy (n = 3), 6 Gy (n = 9) or 6 Gy + rapamycin (n = 4) mice 2 weeks after treatment.
(**E**) Mice were irradiated with 6 Gy or left untreated. 2 weeks thereafter HSCs were sorted based on SA-β-gal staining intensity to isolate non-senescent (SA-β-gal^{low}) and senescent HSCs (SA-β-gal^{high}).
(**F**) As described in (E): Representative raw data showing the size distribution of SA-β-gal^{high} and SA-β-gal^{low} HSCs from sub-lethally irradiated (6 Gy) and control mice.
(**G**) As described in (E): Mean volume (fL) of SA-β-gal^{high} and SA-β-gal^{low} HSCs from 6 Gy (n ≥ 5) and control (n = 11) mice as determined by Coulter counter.
(**H**) Percentage of control (n = 3) and sub-lethally irradiated (3 Gy) HSCs treated with vehicle (n = 7) or rapamycin (n = 3) in the $G_{0/1}$ and S/G_2-M phases of the cell cycle as determined by DNA content (Hoechst 33342) analysis.
(**I**) Percentage of control (n = 7) and sub-lethal irradiated (3 Gy) HSCs that were positive for EdU incorporation from mice treated with vehicle (n = 5) or rapamycin (n = 3).
(**J**) Example of tail DNA measurement by CometChip assay to assess the degree DNA damage.
(**K**) Relative lineage distribution (lymphoid lineage B220, CD3e; myeloid lineage Mac1, Gr-1) of peripheral white blood cells from mice that were untreated or 3 Gy irradiated and afterwards treated with vehicle or rapamycin for 2 weeks (n = 4).
(**L**) Reconstitution from Fig. 1C: Percentage of donor-derived total white blood cells (all CD45.2), B-cells (CD45.2 B220), T-cell (CD45.2 CD3e) and myeloid cells (CD45.2 Mac1, Gr-1) at day 60 post transplantation.
(**M**) Donor (CD45.2) mice were treated with rapamycin or vehicle for 2 weeks, then sub-lethally irradiated (5 Gy) and treated with rapamycin (RAP) or vehicle for another 2 weeks before CD45.2 HSCs were isolated and transplanted into lethally irradiated recipient mice with CD45.1 supporting BM (420,000) (n; donors = 3, recipients = 3). Recipient mice were not treated with rapamycin after the reconstitution. Percentage (%) of donor-derived white blood cells in recipients and slope of the reconstitution kinetics were measured over time.

For all panels, statistical significance was calculated using unpaired t-test to compare 2 samples, one-way ANOVA - multiple comparison - Tukey post-hoc test to compare multiple (3 or more) samples, ****P < 0.0001, ***P < 0.001, **P < 0.01, *P < 0.05; NS, not significant. Mean ± s.d is displayed.

Figure S2

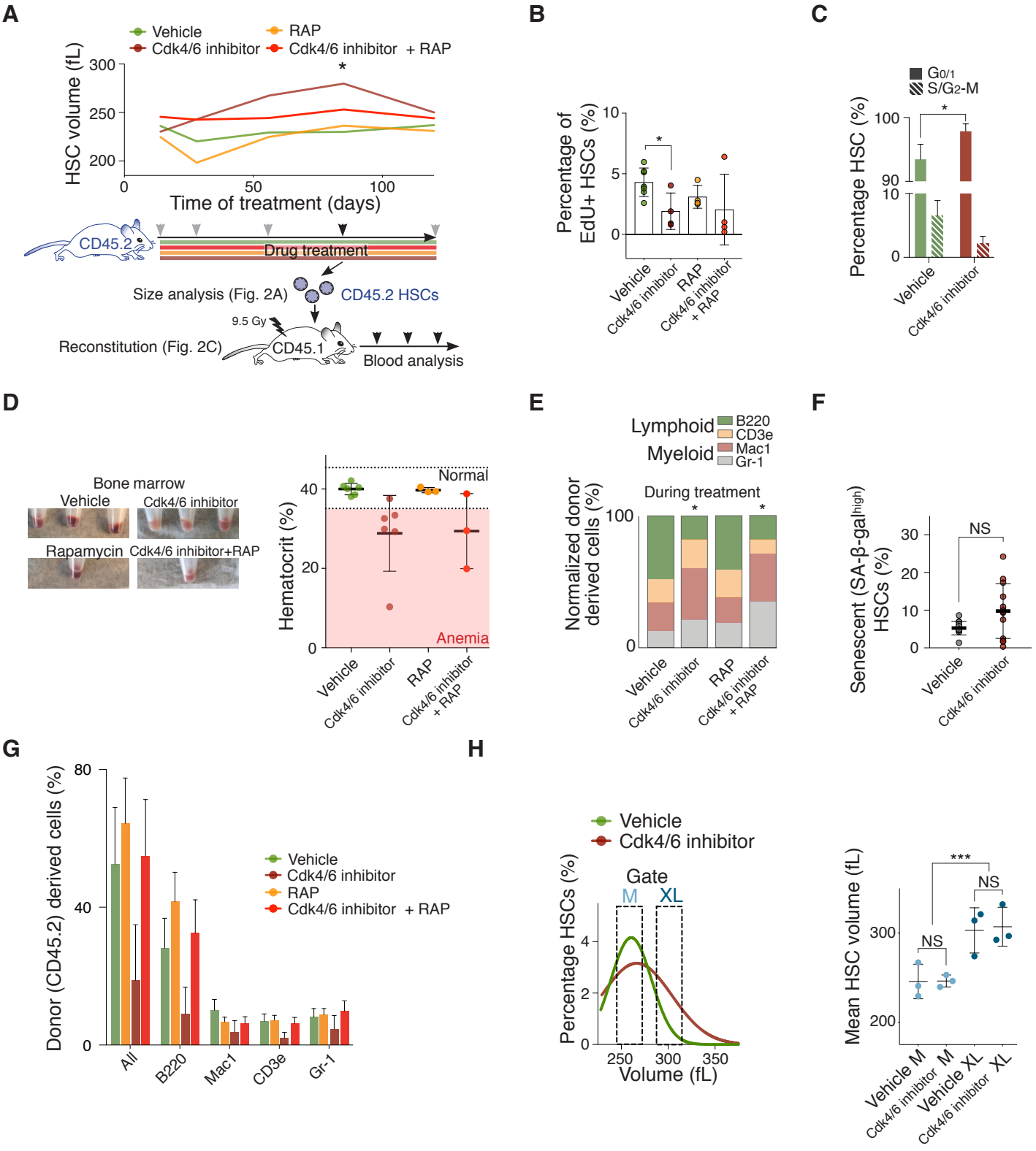
A
Vehicle
Cdk4/6 inhibitor
RAP
Cdk4/6 inhibitor + RAP
HSC volume (fL)
Time of treatment (days)
CD45.2
Drug treatment
Size analysis (Fig. 2A)
CD45.2 HSCs
9.5 Gy
Reconstitution (Fig. 2C)
CD45.1
Blood analysis
B
Percentage of EdU+ HSCs (%)
C
G0/1
S/G2-M
Percentage HSC (%)
D
Bone marrow
Vehicle
Cdk4/6 inhibitor
Rapamycin
Cdk4/6 inhibitor+RAP
Hematocrit (%)
Normal
Anemia
E
Lymphoid
Myeloid
B220
CD3e
Mac1
Gr-1
During treatment
Normalized donor derived cells (%)
F
Senescent (SA-β-gal[high]) HSCs (%)
NS
G
Donor (CD45.2) derived cells (%)
All
B220
Mac1
CD3e
Gr-1
H
Gate
M
XL
Percentage HSCs (%)
Volume (fL)
Mean HSC volume (fL)
***

Fig. S2: The Cdk4/6 inhibitor palbociclib (PD) enlarges HSCs causing their decline in reconstitution potential

(**A**) Experimental design to artificially enlarge HSCs and subsequent analyses as in Fig. 2. Mean volume (fL) of HSCs of vehicle, Cdk4/6 inhibitor (PD), rapamycin (RAP) or Cdk4/6 inhibitor + RAP treated mice was determined at the indicated time points using Coulter counter (grey and black arrows; total treatment time 165 days).
(**B**) Percentage of HSCs from mice during the treatment with vehicle (n = 7), Cdk4/6 inhibitor (PD, n = 4), rapamycin (RAP, n = 4) or Cdk4/6 inhibitor + RAP (n = 4) that were positive for EdU incorporation. Same control as in Fig. S1I.
(**C**) DNA content analysis of HSCs from mice during the treatment with vehicle or PD using Hoechst-33342 (n = 3). Same control as in Fig. S1H.
(**D**) Representative images of bone marrow isolated from mice treated with vehicle, Cdk4/6 inhibitor (PD), rapamycin (RAP) or Cdk4/6 inhibitor + RAP for 85 days. The pale color of the bone marrow indicates anemia. Erythrocyte quantification represented as hematocrit of mice treated with vehicle (n = 6), Cdk4/6 inhibitor (PD, n = 6), rapamycin (RAP, n = 3) or PD + RAP (n = 3). Normal range (35.1 - 45.4 %); anemia (below 35.1 %). Photo credit: Jette Lengefeld, MIT.
(**E**) *In vivo* differentiation assay: Relative lineage distribution (lymphoid lineage B220, CD3e; myeloid lineage Mac1, Gr-1) of peripheral donor-derived (CD45.2) white blood cells during 85-day treatment with vehicle (n = 4), Cdk4/6 inhibitor (PD, n = 4), rapamycin (RAP, n = 4) or Cdk4/6 inhibitor + RAP (n = 4).
(**F**) Percentage of SA-β-gal^{high} HSCs (%) of mice treated with vehicle (n = 12) or Cdk4/6 inhibitor (PD, n = 13, Welch's t-test). Same control as in Fig. S1D.
(**G**) Reconstitution from Fig. 2C: Percentage of donor-derived total white blood cells (all CD45.2), B-cells (CD45.2 B220), T-cell (CD45.2 CD3e) and myeloid cells (CD45.2 Mac1, Gr-1) at day 60 post transplantation.
(**H**) Size distribution of HSCs from mice treated with vehicle or Cdk4/6 inhibitor (PD) for 85 days. Gates used to isolate medium (M) and large (XL) HSCs are indicated. Mean volume (fL) of HSCs from mice treated with vehicle or Cdk4/6 inhibitor (PD) isolated using the M or XL gates was measured using a Coulter counter (n = 3).

For all panels, statistical significance was calculated using unpaired t-test to compare 2 samples, one-way ANOVA - multiple comparison - Tukey post-hoc test to compare multiple (3 or more) samples or otherwise specified, ****$P < 0.0001$, ***$P < 0.001$, **$P < 0.01$, *$P < 0.05$; NS, not significant. Mean ± s.d is displayed.

Figure S3

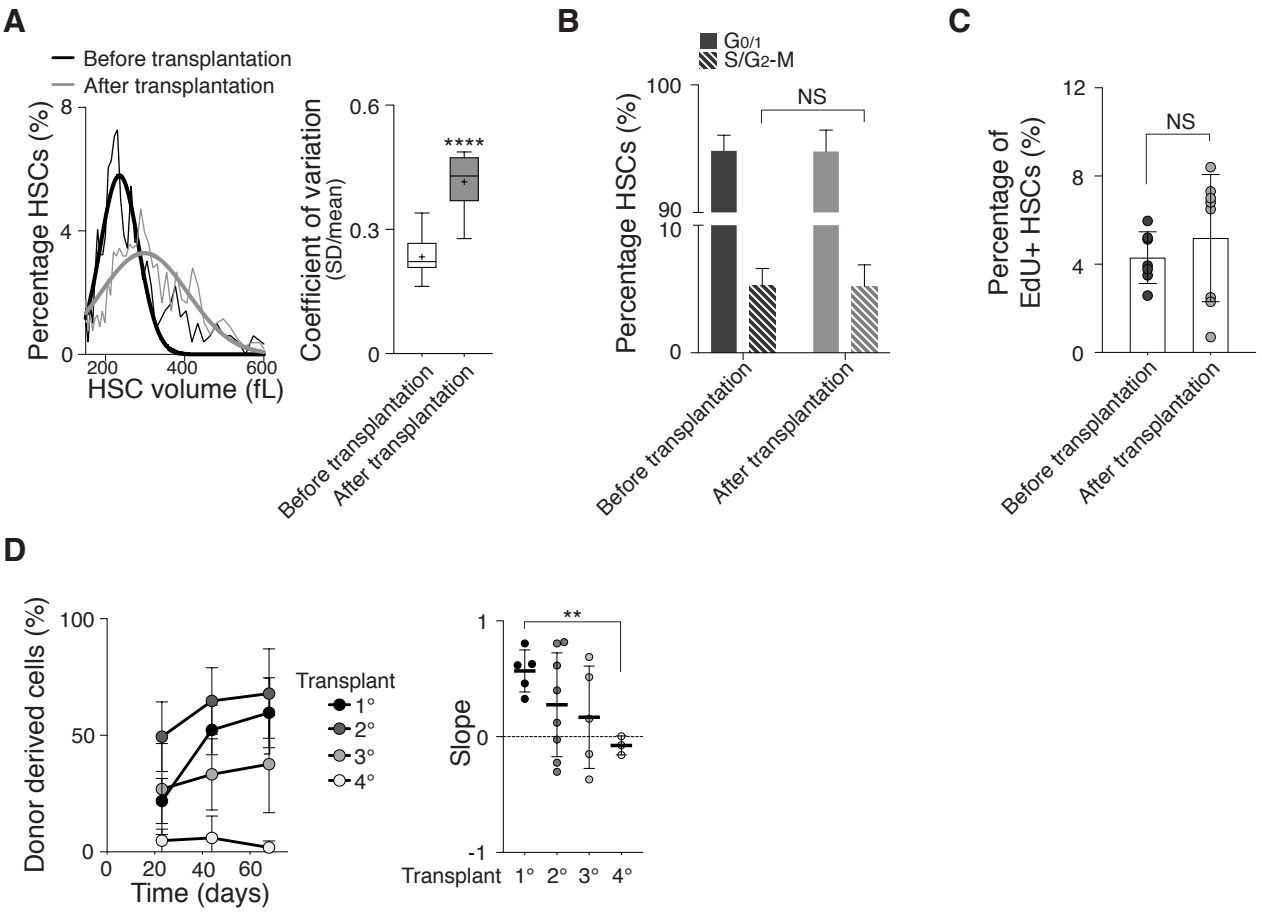

Fig. S3: High cell division frequency enlarges HSCs contributing to their fitness decline

(**A**) Representative raw data showing HSC size distribution: Percentage of HSCs (%) per volume (fL) from before transplantation and after transplantation. Coefficient of variation (CV = SD/mean) of HSCs before transplantation (n = 15) or after transplantation (n = 9). Same control as in Fig. S1C.
(**B, C**) Percentage of HSCs before and 80 days after reconstitution in the $G_{0/1}$ and S/G_2-M phases of the cell cycle as determined by (B) DNA content (Hoechst 33342, n ≥ 3) and (C) EdU incorporation analysis (n ≥ 7, same EdU control as in Fig. S1I).
(**D**) Reconstitution assay: Donor HSCs were used in primary transplant and BM cells from previous transplants for following transplantations. Percentage (%) of donor-derived (CD45.2) white blood cells of primary (1°, n = 5), secondary (2°, n = 8), tertiary (3°, n = 5) and quaternary (4°, n = 3) transplants in recipients and slope of reconstitution kinetics over time.

For all panels, statistical significance was calculated using unpaired t-test to compare 2 samples, one-way ANOVA - multiple comparison - Tukey post-hoc test to compare multiple (3 or more) samples, ****P < 0.0001, ***P < 0.001, **P < 0.01, *P < 0.05; NS, not significant. Mean ± s.d is displayed.

Figure S4

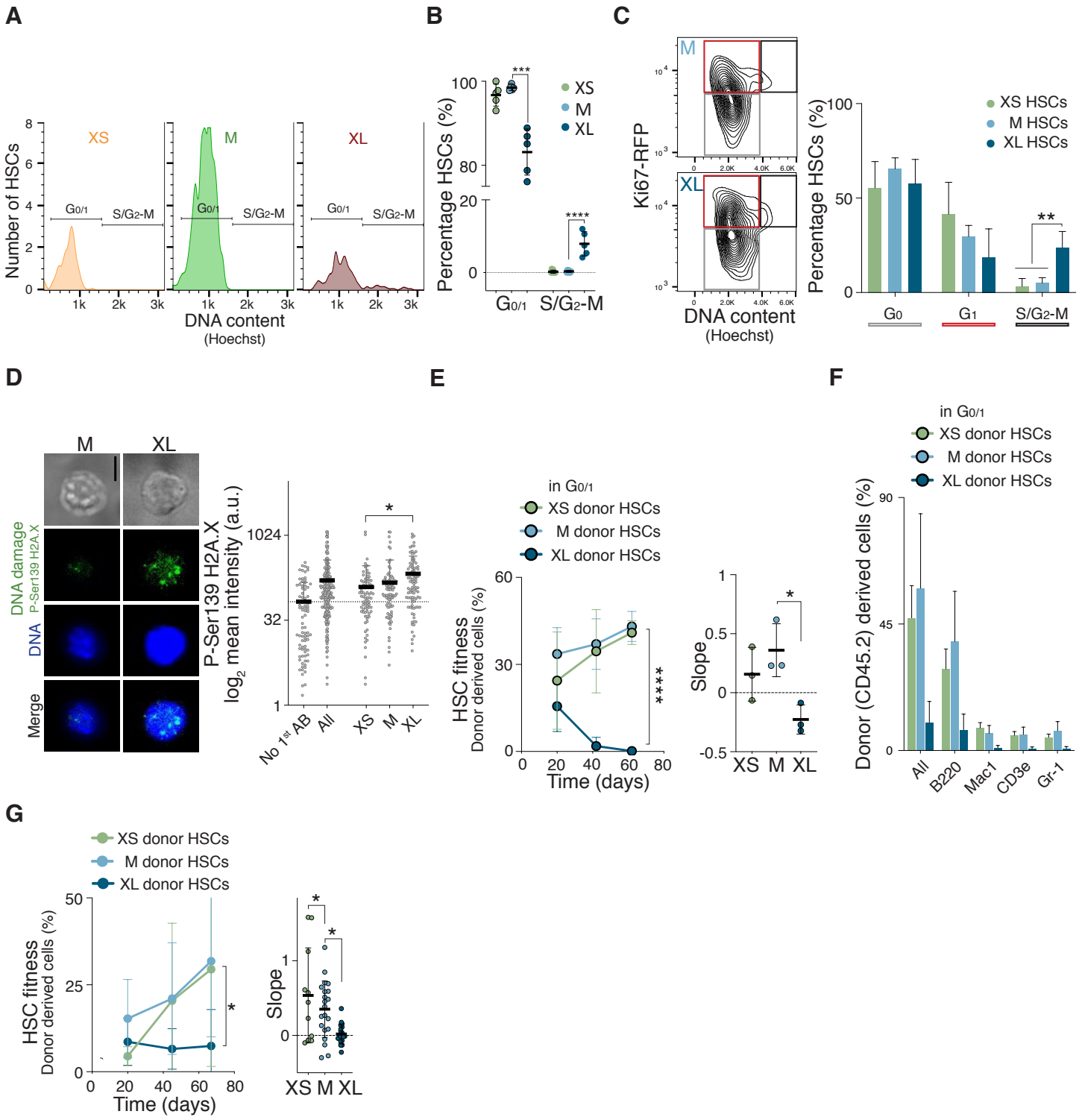
A
XS
M
XL
G0/1
S/G2-M
Number of HSCs
DNA content
(Hoechst)
B
Percentage HSCs (%)
XS
M
XL
G0/1
S/G2-M
C
M
XL
Ki67-RFP
DNA content
(Hoechst)
Percentage HSCs (%)
XS HSCs
M HSCs
XL HSCs
G0
G1
S/G2-M
D
M
XL
DNA damage
P-Ser139 H2A.X
DNA
Merge
P-Ser139 H2A.X
log2 mean intensity (a.u.)
No 1st AB
All
XS
M
XL
E
in G0/1
XS donor HSCs
M donor HSCs
XL donor HSCs
HSC fitness
Donor derived cells (%)
Time (days)
Slope
XS M XL
F
in G0/1
XS donor HSCs
M donor HSCs
XL donor HSCs
Donor (CD45.2) derived cells (%)
All
B220
Mac1
CD3e
Gr-1
G
XS donor HSCs
M donor HSCs
XL donor HSCs
HSC fitness
Donor derived cells (%)
Time (days)
Slope
XS M XL

Fig. S4: Naturally large HSCs are impaired in reconstituting the hematopoietic compartment

(**A**) Representative DNA content analysis of XS-, M- or XL-HSCs using Hoechst-33342. Gates of HSCs in $G_{0/1}$ and S/G_2-M are indicated.
(**B**) Percentage of XS-, M- or XL-HSCs in the $G_{0/1}$ and S/G_2-M phases of the cell cycle as determined by DNA content (Hoechst) analysis ($n \geq 5$).
(**C**) Representative Ki67-RFP and DNA content analysis. The percentage of XS-, M- or XL-HSCs in the G_0, G_1 and S/G_2-M phases of the cell cycle was determined by DNA content (Hoechst 33342) and Ki67-RFP analysis ($n = 4$).
(**D**) Representative images of M- and XL-HSCs stained for P-Ser139 H2A.X (DNA damage) and DAPI (DNA), and quantification of fluorescence mean intensity (a.u., n >100 cells per condition analyzed, scale bar = 5 μm).
(**E**) Reconstitution assay: Percentage of donor-derived (CD45.2) white blood cells in recipient mice after transplantation of $G_{0/1}$ Vybrant™ DyeCycle™ Violet (VD) stain-labelled donor XS-HSCs, M-HSCs or XL-HSCs together with CD45.1 BM (420,000) over time. Slope of percentage (%) of donor-derived white blood cells in recipient over time (n; donors = 3, recipients = 3).
(**F**) Reconstitution from Fig. 5F: Percentage of donor-derived total white blood cells (all CD45.2), B-cells (CD45.2 B220), T-cell (CD45.2 CD3e) and myeloid cells (CD45.2 Mac1, Gr-1) at day 60 post transplantation.
(**G**) Reconstitution assay: Percentage of donor-derived (CD45.2) white blood cells in recipients after transplantation of donor XS-HSCs (n; donors = 10, recipients = 11), M-HSCs (n; donors = 15, recipients = 21) or XL-HSCs (n; donors = 15, recipients = 19) together with CD45.1 BM (420,000) over time. HSCs were not stained with a DNA dye in this experiment. Slope of percentage (%) of donor-derived white blood cells in recipient over time.

For all panels, statistical significance was calculated using unpaired t-test to compare 2 samples, one-way ANOVA - multiple comparison - Tukey post-hoc test to compare multiple (3 or more) samples, ****$P < 0.0001$, ***$P < 0.001$, **$P < 0.01$, *$P < 0.05$; NS, not significant. Mean ± s.d is displayed.

Figure S5

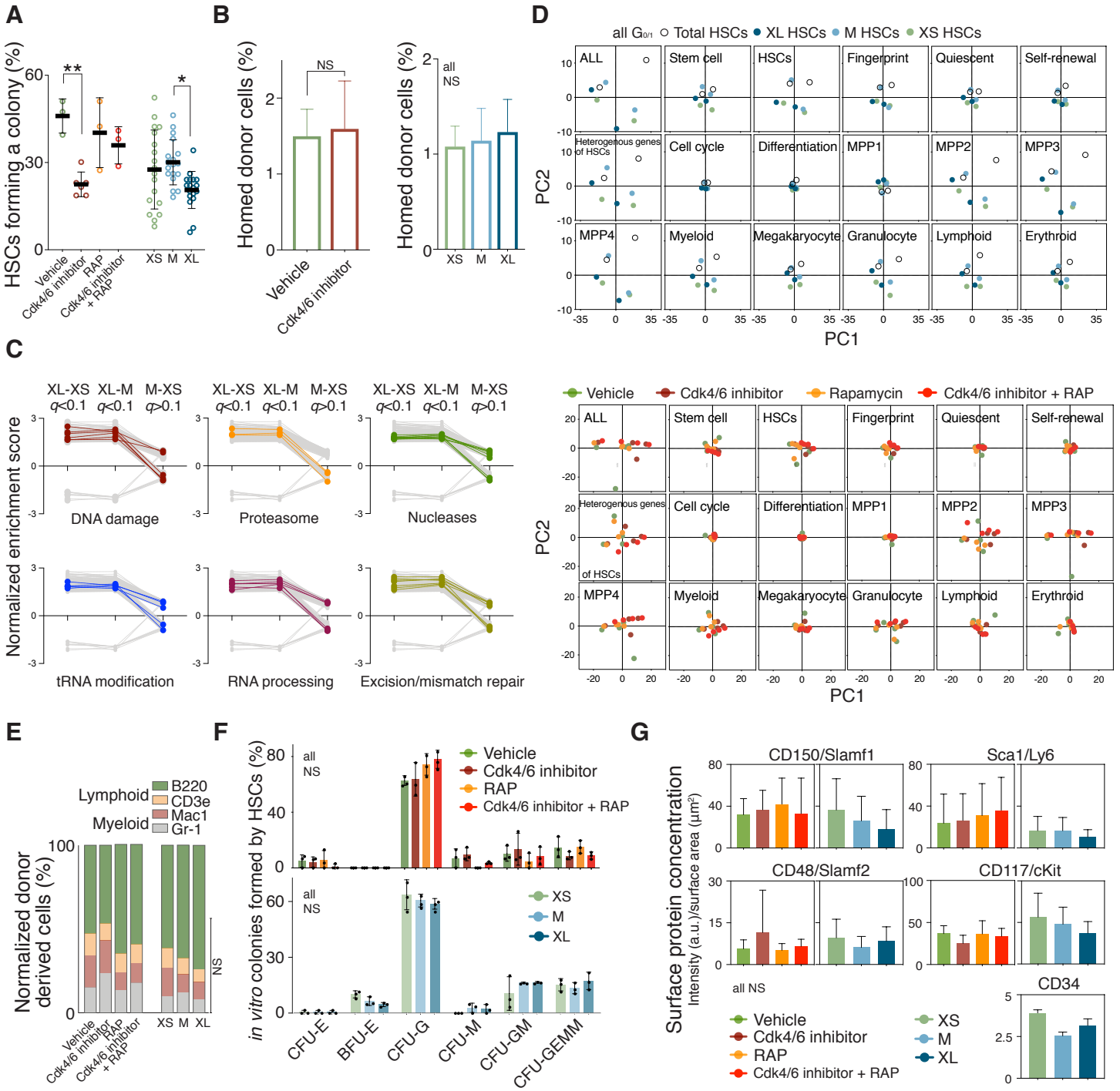
A
HSCs forming a colony (%)
Vehicle
Cdk4/6 inhibitor
RAP
Cdk4/6 inhibitor + RAP
XS M XL
B
Homed donor cells (%)
NS
all NS
C
XL-XS XL-M M-XS
q<0.1 q<0.1 q>0.1
Normalized enrichment score
DNA damage
Proteasome
Nucleases
tRNA modification
RNA processing
Excision/mismatch repair
D
all G0/1 Total HSCs XL HSCs M HSCs XS HSCs
ALL
Stem cell
HSCs
Fingerprint
Quiescent
Self-renewal
Heterogenous genes of HSCs
Cell cycle
Differentiation
MPP1
MPP2
MPP3
MPP4
Myeloid
Megakaryocyte
Granulocyte
Lymphoid
Erythroid
PC1
PC2
Vehicle
Cdk4/6 inhibitor
Rapamycin
Cdk4/6 inhibitor + RAP
E
Lymphoid
B220
CD3e
Myeloid
Mac1
Gr-1
Normalized donor derived cells (%)
NS
F
in vitro colonies formed by HSCs (%)
all NS
Vehicle
Cdk4/6 inhibitor
RAP
Cdk4/6 inhibitor + RAP
XS
M
XL
CFU-E
BFU-E
CFU-G
CFU-M
CFU-GM
CFU-GEMM
G
Surface protein concentration
Intensity (a.u.)/surface area (μm²)
CD150/Slamf1
Sca1/Ly6
CD48/Slamf2
CD117/cKit
CD34
all NS
Vehicle
Cdk4/6 inhibitor
RAP
Cdk4/6 inhibitor + RAP
XS
M
XL

Fig. S5. Large HSCs exhibit reduced capacity of proliferation

(**A**) Colony forming efficiency *in vitro*: HSCs (w/ and w/o Hoechst staining) were isolated from mice treated with vehicle, Cdk4/6 inhibitor (PD), rapamycin (RAP) or Cdk4/6 inhibitor + RAP (n ≥ 3) and XS-, M- or XL-HSCs (n = 18) from untreated WT mice. HSCs were plated onto methylcellulose and the percentage of HSCs forming a colony was quantified. HSCs were not treated with drugs *ex vivo*.
(**B**) Homing assay: HSCs were isolated from mice treated with vehicle, Cdk4/6 inhibitor (PD), rapamycin (RAP) or Cdk4/6 inhibitor + RAP (n = 4) and XS-, M- or XL-HSCs from untreated WT mice (n = 2). The HSCs were transplanted into lethally irradiated recipient mice. Percentage (%) of donor-cells in the bone of recipient mice was measured 21 h after transplantation.
(**C**) GO gene sets were analyzed using GSEA and then filtered to be different ($q < 0.1$) when comparing M- and XS-HSCs with XL-HSCs (all $G_{0/1}$), but indistinguishable ($q > 0.1$) when comparing M-HSCs with XS-HSCs. Biological processes are colored when ≥ 20 % of their GO gene sets passed the filter. Biological processes are displayed in grey when less than 20 % of their GO gene sets passed the filter (Table S1).
(**D**) Expression differences between differently sized $G_{0/1}$ HSCs were assessed on the basis of principle components analysis (PCA) using published HSC genes affecting stem cell identity and differentiation (Table S2). Relative distances were collapsed into two dimensions using PCA. Samples analyzed: $G_{0/1}$ total, XS-, M-, XL HSCs (n = 2, bottom) and vehicle, Cdk4/6 inhibitor (PD), rapamycin (RAP), Cdk4/6 inhibitor + RAP treated HSCs (n = 4, top).
(**E**) *In vivo* differentiation assay: Relative lineage distribution (lymphoid lineage B220, CD3e; myeloid lineage Mac1, Gr-1) from peripheral donor-derived (CD45.2) white blood cells 80 days after recipient mice were reconstituted with HSCs from mice treated with vehicle (n = 8), Cdk4/6 inhibitor (PD, n = 6), RAP (n = 8) or Cdk4/6 inhibitor + RAP (n = 5) or with XS- (n = 5), M- (n = 12), XL- (n = 6) HSCs from WT mice. No drug treatment was performed after the reconstitution.
(**F**) *In vitro* differentiation assay: HSCs from mice treated with vehicle, Cdk4/6 inhibitor (PD), rapamycin (RAP) or Cdk4/6 inhibitor + RAP (top graph) or XS-, M- or XL-HSCs (bottom graph) were plated onto methylcellulose and GEMM, GM or single lineages (G, M and E) colonies were counted (n = 6, representative experiment shown).
(**G**) Fluorescence intensity (a.u.) of CD150/Slamf1, Sca1/Ly6, CD48/Slamf2, CD117/cKit and CD34 per surface area (μm^2) was determined in differently sized HSCs or HSCs isolated from mice treated with vehicle, Cdk4/6 inhibitor (PD), rapamycin (RAP) or Cdk4/6 inhibitor + RAP (n ≥ 3).

For all panels, statistical significance was calculated using unpaired t-test to compare 2 samples, one-way ANOVA - multiple comparison - Tukey post-hoc test to compare multiple (3 or more) samples, ****$P < 0.0001$, ***$P < 0.001$, **$P < 0.01$, *$P < 0.05$; NS, not significant. Mean ± s.d is displayed.

Figure S6

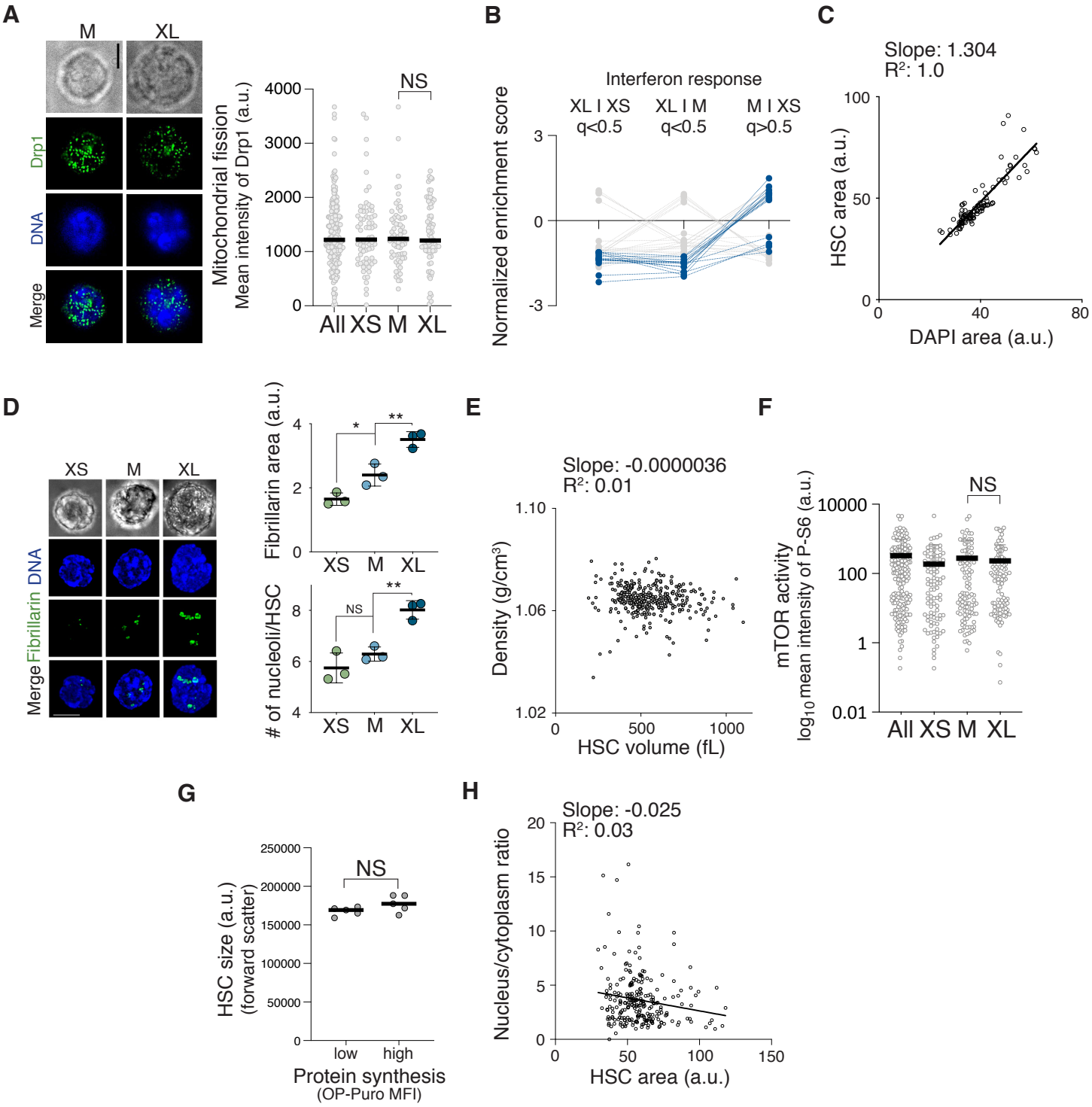
A
M
XL
Drp1
DNA
Merge
Mitochondrial fission
Mean intensity of Drp1 (a.u.)
NS
All XS M XL
B
Interferon response
XL I XS
q<0.5
XL I M
q<0.5
M I XS
q>0.5
Normalized enrichment score
C
Slope: 1.304
R²: 1.0
HSC area (a.u.)
DAPI area (a.u.)
D
XS M XL
Merge Fibrillarin DNA
Fibrillarin area (a.u.)
# of nucleoli/HSC
NS
E
Slope: -0.0000036
R²: 0.01
Density (g/cm³)
HSC volume (fL)
F
mTOR activity
log10 mean intensity of P-S6 (a.u.)
NS
All XS M XL
G
HSC size (a.u.)
(forward scatter)
NS
low high
Protein synthesis
(OP-Puro MFI)
H
Slope: -0.025
R²: 0.03
Nucleus/cytoplasm ratio
HSC area (a.u.)

Fig. S6. Large HSCs exhibit altered metabolism

(**A**) Mitochondrial fission: Representative images of all, XS-, M- and XL-sized $G_{0/1}$ HSCs stained for Drp1 and DNA (DAPI) and quantification of fluorescence mean intensity Drp1 (a.u., n > 70 cells per condition analyzed).
(**B**) Interferon response associated GO gene sets were analyzed using GSEA. Blue colored GO gene sets passed the filter to be different (q < 0.5) when comparing M- and XS-HSCs with XL-HSCs, but indistinguishable (q > 0.5) when comparing M-HSCs with XS-HSCs. Interferon response associated GO gene sets that did not pass the filter are displayed gray.
(**C**) Nucleus size correlates with HSC size: HSC area (a.u.) plotted vs. DAPI area (a.u.).
(**D**) Representative images of XS-, M- and XL-sized HSCs from WT mice stained for fibrillarin and DNA (DAPI, scale bar is 5 μm). Quantification of total fibrillarin area (a.u.) and number (#) of nucleoli of XS-, M- and XL-sized HSCs (n > 100 HSCs per condition analyzed).
(**E**) HSCs were expanded *in vitro* for 2 days and the density (g/cm^3) per HSC volume (fL) quantified (n = 351).
(**F**) mTOR activity: Quantification of fluorescence mean intensity P-S6 (a.u., n > 100 cells per condition analyzed).
(**G**) Protein synthesis and size: Size (forward scatter) of HSCs that were analyzed for protein synthesis using OP-Puro mean fluorescence intensity (a.u., n = 5).
(**H**) Nucleus:cytoplasm ratio (C/V) per HSC area (a.u.) quantified (n = 250).

For all panels, statistical significance was calculated using unpaired t-test to compare 2 samples, one-way ANOVA - multiple comparison - Tukey post-hoc test to compare multiple (3 or more) samples, ****P < 0.0001, ***P < 0.001, **P < 0.01, *P < 0.05; NS, not significant. Mean ± s.d is displayed.

Figure S7

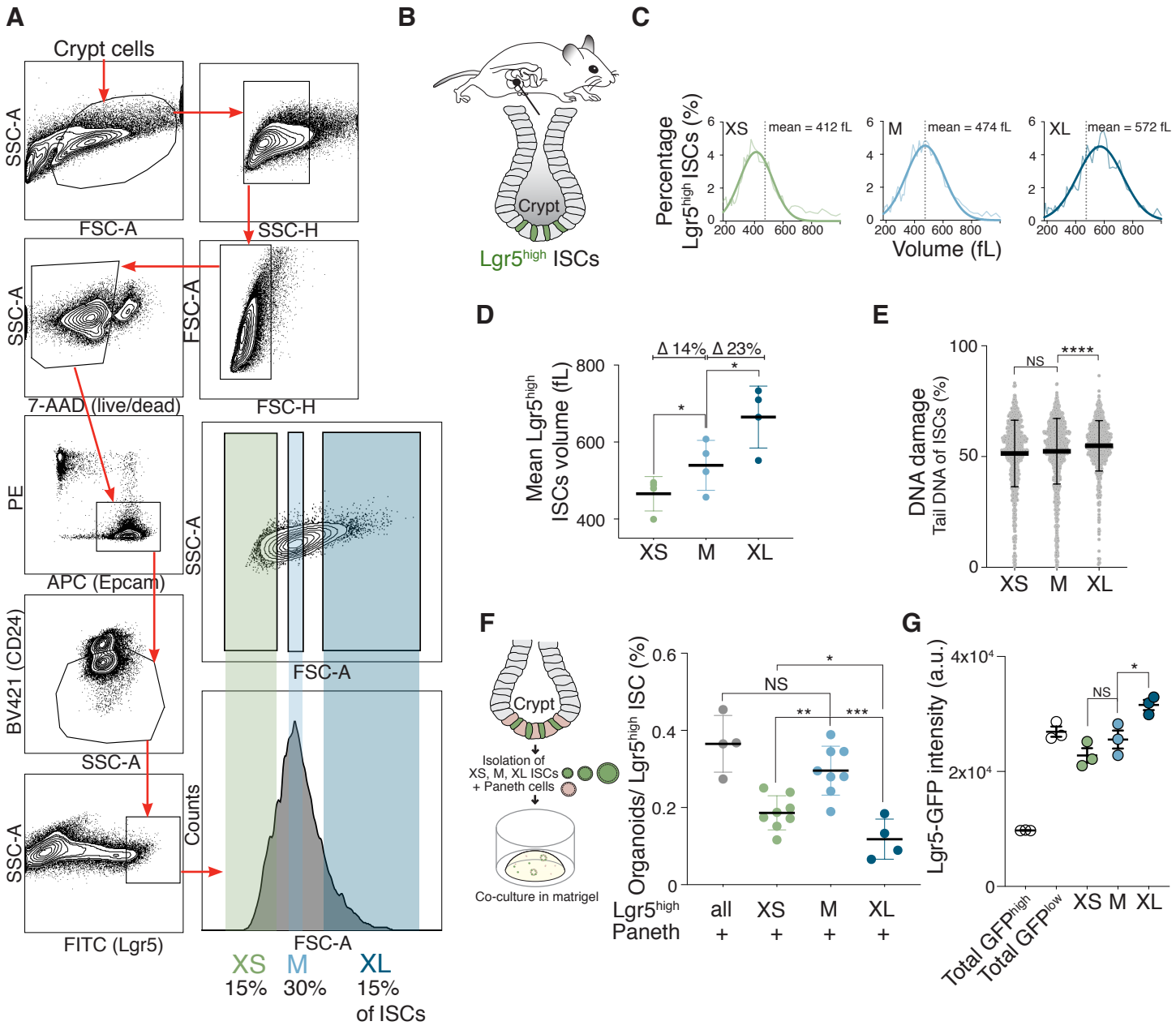
A
Crypt cells
SSC-A
FSC-A
SSC-H
FSC-H
7-AAD (live/dead)
PE
APC (Epcam)
BV421 (CD24)
FITC (Lgr5)
Counts
XS 15%
M 30%
XL 15% of ISCs
B
Crypt
Lgr5high ISCs
C
Percentage Lgr5high ISCs (%)
XS mean = 412 fL
M mean = 474 fL
XL mean = 572 fL
Volume (fL)
D
Mean Lgr5high ISCs volume (fL)
Δ 14%
Δ 23%
E
DNA damage Tail DNA of ISCs (%)
NS
****
F
Isolation of XS, M, XL ISCs + Paneth cells
Co-culture in matrigel
Organoids/ Lgr5high ISC (%)
Lgr5high Paneth
all
G
Lgr5-GFP intensity (a.u.)
Total GFPhigh
Total GFPlow

Fig. S7: The size of intestinal stem cells predicts their proliferation potential

(**A**) Sorting protocol used to isolate ISCs from 8 week-old mice. Representative FACS plots of crypt cells to enrich for ISCs (Epcam+, CD24-, Lgr5^{high}) are shown. Histogram on the right shows the gates used to isolate small (XS), medium (M) and large (XL) ISCs.
(**B**) Schematic location of Lgr5^{high} intestinal stem cells (ISCs) in the small intestine.
(**C**) Cell volume (fL) of XS-, M- or XL-ISCs was measured with a Coulter counter. Gaussian fit was used to determine mean cell volume.
(**D**) Mean volume (fL) of ISCs isolated using the XS, M or XL gates as measured by Coulter counter ($n = 4$, Δ = difference).
(**E**) CometChip assay to measure DNA damage: Percentage tail DNA of XS-, M- and XL- sized ISCs ($n \geq 729$).
(**F**) Percentage of organoids formed by all ($n = 4$), XS- ($n = 8$), M- ($n = 8$) or XL- ($n = 4$) Lgr5^{high} ISCs co-cultured with Paneth cells.
(**G**) Lgr5-GFP intensity (a.u.) of XS-, M- and XL-ISCs and total ISCs with high and low GFP intensity ($n = 3$).

For all panels, statistical significance was calculated using unpaired t-test to compare 2 samples, one-way ANOVA - multiple comparison - Tukey post-hoc test to compare multiple (3 or more) samples, ****$P < 0.0001$, ***$P < 0.001$, **$P < 0.01$, *$P < 0.05$; NS, not significant. Mean ± s.d is displayed.

Figure S8

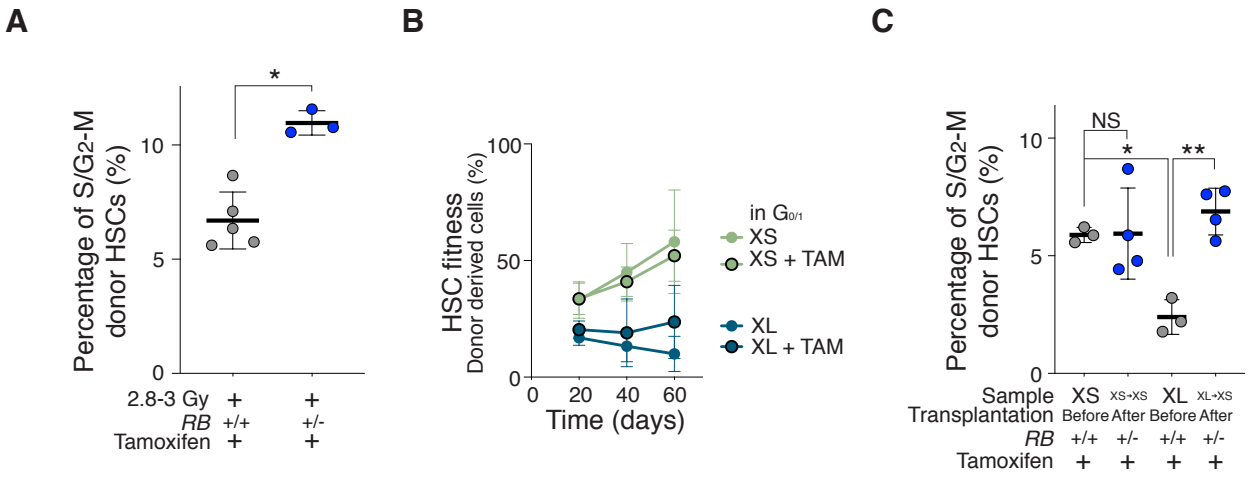

Fig. S8: Reducing the size of large HSCs restores their reconstitution potential

(**A**) Percentage of 2.8 Gy irradiated *RB+/+* (n = 5) or *RB +/-* (n = 3) HSCs that are in S/G2-M from reconstituted animals as determined by DNA content (Hoechst 33342) analysis 60 days after reconstitution.
(**B**) 600 differently sized donor-derived HSCs together with CD45.1 supporting BM cells (420,000) were transplanted into lethally irradiated recipient mice. Percentage (%) of donor-derived white blood cells in recipients after transplantation of G0/1 XS-HSCs (n; donors = 5, recipients = 6), or G0/1 XL-HSCs (n; donors = 5, recipients n = 6) treated with or without tamoxifen over time. Same data as in Fig. 5F and 7F.
(**C**) Percentage of S/G2-M XS or XL *RB+/+* HSCs (%) was determined (before transplantation).
XS or XL *RB+/fl* HSCs were transplanted into lethally irradiated mice, which were treated with tamoxifen to excise the floxed *RB* allele of HSCs and reduce their size. 60 days after reconstitution, size-reduced donor XS->XS or XL->XS *RB+/-* HSCs were evaluated for percentage of S/G2-M (after transplantation).

For all panels, statistical significance was calculated using unpaired t-test to compare 2 samples, one-way ANOVA - multiple comparison - Tukey post-hoc test to compare multiple (3 or more) samples, ****P < 0.0001, ***P < 0.001, **P < 0.01, *P < 0.05; NS, not significant. Mean ± s.d is displayed.

Figure S9

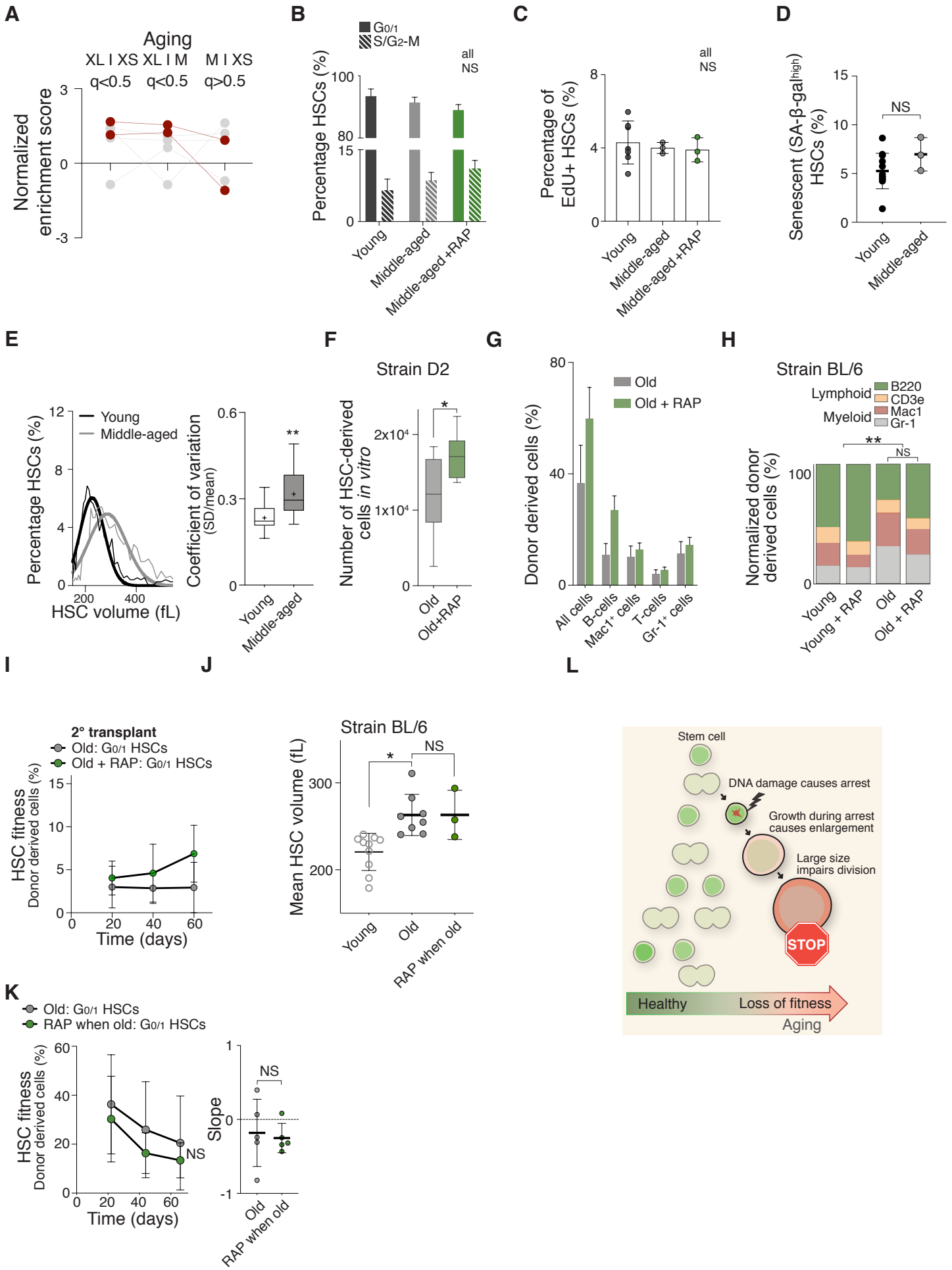
A
Aging
XL I XS XL I M M I XS
q<0.5 q<0.5 q>0.5
Normalized enrichment score
B
G0/1
S/G2-M
all
NS
Percentage HSCs (%)
Young
Middle-aged
Middle-aged+RAP
C
all
NS
Percentage of EdU+ HSCs (%)
Young
Middle-aged
Middle-aged+RAP
D
NS
Senescent (SA-β-gal high) HSCs (%)
Young
Middle-aged
E
Young
Middle-aged
Percentage HSCs (%)
HSC volume (fL)
Coefficient of variation (SD/mean)
**
Young
Middle-aged
F
Strain D2
*
Number of HSC-derived cells in vitro
Old
Old+RAP
G
Old
Old + RAP
Donor derived cells (%)
All cells
B-cells
Mac1+ cells
T-cells
Gr-1+ cells
H
Strain BL/6
Lymphoid
Myeloid
B220
CD3e
Mac1
Gr-1
**
NS
Normalized donor derived cells (%)
Young
Young + RAP
Old
Old + RAP
I
2° transplant
Old: G0/1 HSCs
Old + RAP: G0/1 HSCs
HSC fitness
Donor derived cells (%)
Time (days)
J
Strain BL6
*
NS
Mean HSC volume (fL)
Young
Old
RAP when old
L
Stem cell
DNA damage causes arrest
Growth during arrest causes enlargement
Large size impairs division
STOP
Healthy
Loss of fitness
Aging
K
Old: G0/1 HSCs
RAP when old: G0/1 HSCs
HSC fitness
Donor derived cells (%)
NS
Time (days)
Slope
NS
Old
RAP when old

Fig. S9: Enlargement of HSCs contributes to fitness decline during aging

(**A**) Aging associated GO gene sets were analyzed using GSEA. Red colored GO gene sets passed the filter to be different ($q < 0.5$) when comparing M- and XS-HSCs with XL-HSCs, but indistinguishable ($q > 0.5$) when comparing M-HSCs with XS-HSCs. Aging associated GO gene sets that did not pass the filter are displayed gray.
(**B, C**) HSCs from young (5-9 wks, n = 3-7), middle-aged (56-65 wks, n = 3) or middle-aged + rapamycin (56-65 wks, n = 3) BL/6 mice in the $G_{0/1}$ and S/G_2-M phase of the cell cycle as determined by DNA (Hoechst) content analysis (B) or EdU incorporation (C). Same control as in Fig. S1H (Hoechst) and S1I (EdU).
(**D**) Percentage of SA-β-gal^{high} HSCs (%) from young (n = 12) and old (n = 3) mice. Same control as in Fig. S1D.
(**E**) Representative raw data showing size distribution: Percentage of HSCs (%) per volume (fL) from young or middle-aged mice. Coefficient of variation (CV = SD/mean) of HSCs from young (n = 15) or middle-aged (n = 10) BL/6 mice. Same control as in Fig. S1C.
(**F**) Colony forming efficiency *in vitro*: HSCs from D2 mice treated with vehicle or rapamycin during aging were plated on methylcellulose and cell number was quantified (n = 9).
(**G**) Reconstitution from Fig. 8E: Percentage of donor-derived total white blood cells (all CD45.2), B-cells (CD45.2 B220), T-cell (CD45.2 CD3e) and myeloid cells (CD45.2 Mac1, Gr-1) at day 60 post transplantation.
(**H**) *In vivo* differentiation assay: Relative lineage distribution (lymphoid lineage B220, CD3e; myeloid lineage Mac1, Gr-1) from peripheral donor-derived (CD45.2) white blood cells 80 days after recipients were reconstituted with HSCs from 8 (young) or 102 (old) week-old BL6 mice treated with vehicle or RAP. No drug treatment was performed after the reconstitution (n = 4).
(**I**) Secondary transplant: Lethally irradiated recipient mice (CD45.1) were reconstituted with CD45.1 BM cells (420,000) and donor (CD45.2)-derived $G_{0/1}$ HSCs from primary transplant (Fig. 8E, n; donors = 5, recipients = 5), for which donor old (86-102 wks) BL/6 mice treated with vehicle or rapamycin during their life. Percentage (%) of donor-derived white blood cells.
(**J**) Mean volume (fL) of HSCs from 5-9 week old (young, n = 9), 86-102 week old ($G_{0/1}$ old, n = 8) or old mice treated with rapamycin for 2-3 month starting at week 77 ($G_{0/1}$ RAP, n = 3) BL/6 mice was measured using a Coulter counter. Same young and old data as in Fig. 8B.
(**K**) Reconstitution assay: Lethally irradiated recipient mice (CD45.1) were reconstituted with CD45.1 BM cells (420,000) and donor (CD45.2)-derived $G_{0/1}$ HSCs from old (86 wks) BL/6 mice treated with rapamycin (n; donors = 5, recipients = 5) for 2-3 months during old age (week 77 onwards) or untreated (n; donors = 5, recipients = 5). Percentage (%) of donor-derived white blood cells and slope of the reconstitution kinetics over time in recipients.
(**L**) Model for how HSC enlargement contributes to their functional decline with age. With age, HSCs are more likely to have encountered stochastic cellular damage during divisions. This DNA damage causes transient cell cycle arrests, during which mTOR continues to promote cellular growth and enlarges HSCs. This enlargement reduces the ability of HSCs to build a blood system.

For all panels, statistical significance was calculated using unpaired t-test to compare 2 samples, one-way ANOVA - multiple comparison - Tukey post-hoc test to compare multiple (3 or more) samples, ****$P < 0.0001$, ***$P < 0.001$, **$P < 0.01$, *$P < 0.05$; NS, not significant. Mean ± s.d is displayed.

Table legends

Table S1: Gene Set Enrichment Analysis of expression in differently sized HSCs
GO gene sets were analyzed using GSEA and then filtered to be different ($q < 0.1$) when comparing M- and XS-HSCs with XL-HSCs (all $G_{0/1}$), but indistinguishable ($q > 0.1$) when comparing M-HSCs with XS-HSCs or filtered to be different ($q < 0.1$) when comparing PD with PD+RAP, rapamycin and vehicle, but indistinguishable ($q > 0.1$) when comparing PD+RAP, vehicle and rapamycin.

Table S2: Gene set collection
Published lists of gene categories related to HSC identity and differentiation used for analysis.

Table S3: Differentially expressed genes
Differentially expressed genes of published categories related to HSC identity and differentiation when comparing vehicle, Cdk4/6 inhibitor (PD), rapamycin (RAP) and Cdk4/6 inhibitor + RAP treatments or $G_{0/1}$ XS-, M- and XL-HSCs from untreated WT mice.

Materials and Methods

Mice

All work was performed in accordance with the MIT Institutional Animal Care Facility and with guidelines at Massachusetts Institute of Technology (*IACUC*) (protocol number: 0715-073-18, 0718-053-21).

Unless otherwise indicated, all experiments were performed with female C57BL/6J (BL/6) mice 8-12 weeks. 9-11 wks old B6.SJL-*Ptprc*^{a}*Pepc*^{b}/BoyJ (CD45.1, B6.SJL, JAX stock #002014) and 8-12 wks old C57BL/6J mice (CD45.2, JAX stock #000664) for reconstitution assays were purchased from The Jackson Laboratory (Bar Harbor, ME). Female DBA/2J (D2) mice (JAX stock #000671, Charles River stock #026) were used for aging studies as indicated. Lgr5-EGFP-IRES-CreERT2 mice (B6.129P2-Lgr5tm1(cre/ERT2)Cle/J, JAX stock #008875) were used for ISC isolation. The Ki67^{RFP} knock-in strain (Jax stock # 029802, *Mki67*$^{tm1.1Cle}$/J) was used to determine cell cycle stages. *Rosa26CreERT2* mice (*80*) (B6.129- *Gt(ROSA) 26Sortm1 (cre/ERT2) Tyj*/J, JAX stock #008463) were crossed with *TSC1*$^{fl/fl}$ mice (*81*) (*Tsc1tm1Djk*/J, JAX stock #005680) to generate strain *TSC1*$^{fl/fl}$*;R26-creERT2*. *RB*$^{fl/+}$ (*Rb1*^{tm2Brn}/J, JAX stock #026563, (*82*) were crossed with *Rosa26CreERT2* mice (B6.129- *Gt(ROSA) 26Sortm1 (cre/ERT2) Tyj*/J, JAX stock #008463) to generate *RB*$^{fll+}$*; R26-creERT2* mice, which were used at week 8. *R26-rtTA tetO-H2B-GFP* (Jax stock #005104 and #006965) mice were created by crossing and GFP expression was induced using doxycycline food (Envigo, TD.01306).

HSC isolation and measurements

Murine bone marrow (BM)-derived HSCs were isolated as described previously (*69*). Briefly, BM was harvested by flushing the long bones. Red blood cells were lysed in ammonium-chloride-potassium (ACK) buffer and samples were washed in Iscove's Modified Dulbecco's Medium (IMDM) containing 2 % fetal bovine serum (FBS). Lineage positive cells were depleted using a mouse lineage cell depletion kit and the following antibodies from were used for staining: Rat monoclonal PE/Cy7 anti-mouse CD150, BioLegend, Cat#115913; RRID: AB_439796; Rat monoclonal PE anti-mouse CD150, BioLegend, Cat#115904; RRID: AB_313683; Armenian hamster monoclonal BV421 anti-mouse CD48, BioLegend, Cat#103427; RRID: AB_10895922; Armenian hamster monoclonal APC/Cy7 anti-mouse CD48, BioLegend, Cat#103431; RRID: AB_2561462; Rat monoclonal PE/Cy7 anti-mouse Ly-6A/E, BioLegend, Cat#108114; RRID: AB_493596; Rat monoclonal APC anti-mouse CD117, BioLegend, Cat#105812; RRID: AB_313221; Rat monoclonal PE anti-mouse CD150, BD Biosciences, Cat#562651; RRID: AB_2737705; Rat monoclonal FITC anti-mouse Ly-6A/E, BD Biosciences, Cat#562058; RRID: AB_10898185; Rat monoclonal PE/Cy7 anti-mouse Ly-6A/E, BioLegend, Cat#108114; RRID: AB_493596; Rat monoclonal PE/Cy5 anti-mouse CD150, BioLegend, Cat#115911; RRID: AB_493599; Armenian hamster monoclonal FITC anti-mouse CD48, BioLegend, Cat# 103404; RRID: AB_313019; Rat monoclonal APC anti-mouse CD117, BD Biosciences, Cat#561074; RRID: AB_10563203. 7-AAD or propidium iodide was used for the identification of non-viable cells. Cells were sorted using an Aria cell sorter (Becton Dickinson).

Human BM samples were purchased from AllCells®, which guidelines follow strictly the need for informed consent. HSCs were purified as described previously (*70, 83*). Briefly, BM was diluted with Ficoll buffer (2 mM EDTA in phosphate-buffered saline (PBS)) at a ratio of 7:1. Mixtures were carefully layered over Ficoll-Paque Premium (Sigma, GE17-5442-02) at a ratio of 3:1 in a conical tube and centrifuged at 400 x g at 18°C for 35 min. The upper layer containing plasma and platelets was aspirated leaving the

mononuclear cell layer undisturbed at the interphase. The mononuclear cell layer was mixed gently with Ficoll buffer and centrifuged at 300 x g at 18°C for 10 min. Cells were washed with 40 mL of Ficoll buffer and centrifuged at 200 x g at 18°C for 10 min. Cells were resuspended in 300 µL MACS buffer (2 mM EDTA, 5 mg/mL bovine serum albumin (BSA) in PBS) per 10^8 cells. 100 µL of FcR Blocking Reagent (Miltenyi Biotec, 130-059-901) per 10^8 cells and 100 µL of CD34 MicroBeads (Miltenyi Biotec, 130-046-702) per 10^8 cells were added. For staining, cells were incubated with the following antibodies for 30 min at 4°C: Mouse APC anti-human Lineage Cocktail (CD3, CD14, CD16, CD19, CD20, CD56) BioLegend, Cat#348803; mouse monoclonal FITC anti-human CD90, BD Biosciences, Cat#561969; RRID: AB_10895382; Rat monoclonal PE-Cy5 anti-human CD49f, BD Biosciences, Cat#551129; RRID: AB_394062; Mouse monoclonal PE-Cy7 anti-human CD45RA, BD Biosciences, Cat#560675; RRID: AB_1727498; Mouse monoclonal PE anti-human CD38, BD Biosciences, Cat#342371; RRID: AB_400453. HSCs were purified using a LS MACS Column in a magnetic separator, resuspended in IMDM with 5 % FBS and sorted using an Aria cell sorter (Becton Dickinson).

Cell cycle stage analysis

BM cells were resuspended at 10^6 cells/mL in pre-warmed IMEM supplemented with 2 % FBS and 6.6 µg/mL Hoechst-33342 (Thermo Fisher Scientific, #H3570). After 45 min of incubation at 37°C in a water-bath, cells were washed with cold IMEM supplemented with 2 % FBS and kept at 4°C. Lineage positive cells were depleted and remaining cells stained using HSCs antibodies as described above. Because Hoechst-33342 can be toxic to cells, we also used the Vybrant™ DyeCycle™ Violet Stain (Thermo Fisher, #V35003) to stain DNA (5 µM, 10^6 cells/mL) by incubating cells at room temperature (RT) for 30 min. Cells were not washed before cytometer analysis and sorting. To distinguish between G_0 and G_1 HSCs, we took advantage of transgenic Ki67-RFP mice and analyzed HSCs that were stained with Hoechst-33342 as described above using flow cytometry. For *in vivo* proliferation studies, 1.25 mg EdU was injected intraperitoneally into mice 24 h before sacrifice. EdU incorporation into the DNA of HSCs was evaluated according to the manufacturer's instructions with the Click-iT® EdU Alexa Fluor® 488 Imaging Kit.

HSC volume measurements

Size of HSCs was determined using a Multisizer-3 Coulter Counter (Beckman Coulter) or as indicated. When using the forward scatter (FSC-A) of a flow cytometer to isolate HSCs of a specific size, the gates were set so that XS-HSCs encompass the 10 % smallest and XL-HSCs the 10 % largest cells in the HSC population. The M gate was set to isolate HSCs of mean size +/- 10 %. Cytometer-based HSC size fractionation was confirmed by measuring the absolute cell volume using the Coulter Counter. To determine HSC size using the Coulter Counter, HSC size distribution data from Coulter Counter measurements were fitted to a Gaussian distribution to calculate mean size and standard deviation (SD). If needed, bone marrow from test and control animals were frozen in FBS with 10 % DMSO at -80 °C and used for HSC isolation and size analysis later. Size evaluation by microscopy is described in the section entitled "Fluorescence assays".

We also explored using flow cytometry (forward scatter) measurements to assess cell size, but this method was only able to detect large differences in cell size. Forward scatter (FSC-A) measurements are not an accurate method to determine size as several other parameters influence this measurement

(wavelength of laser illumination, collection angle, refractive index of the particle, and flow medium). Thus, FSC-A values can differ between independent experiments making it difficult to compare experiments. We therefore determined the sensitivity and accuracy of the FSC-A size measurement by comparing them to size measurements by Coulter Counter. We calculated a ratio of the mean FSC-A value of experimental and control HSCs. The relationship between the ratio (mean FSC-A experimental/mean control FSC-A) and the percentage enlargement measured by Coulter Counter was not linear. Small increases in cell size where not detected by FSC-A measurement. This result indicates that FSC-A can only detect large differences in HSC volume.

Reconstitution and homing assays

B6.SJL recipient mice (CD45.1) were irradiated with 9.5 Gy using a Cesium-137 irradiator (γ cell 40). Donor HSCs were transplanted 10 h post irradiation. HSCs were transferred under isoflurane anesthesia by retro-orbital injection using 500 live HSCs (C57BL/6J, CD45.2) combined with 420,000 B6.SJL (CD45.1) supporting white blood cells in a volume of 100 µL per mouse. We chose this high number of HSCs in our transplantation experiments to obtain robust reconstitution even when utilizing HSCs with poor reconstitution capacity. For reconstitutions using HSCs from sub-lethally irradiated (3 or 5 Gy) or aged animals, we used 750-1000 HSCs because of their reduced potential to reconstitute lethally irradiated recipient mice.

Reconstituted animals were housed in sterile caging, administered antibiotic septra water and wet food on the floor of their cages and monitored twice daily for 14 days for activity, labored breathing/dyspnea and appearance. One half of the mice cages were placed on a heat mat with power control (QC supplies, 250220, 250230). Reconstitution ability of HSCs was determined 3, 6 and 9 weeks after reconstitution by peripheral blood analysis. Peripheral blood was collected in heparinized capillary tubes into sodium heparin (Sigma-Aldrich, H3149-100KU) diluted in PBS. Red blood cells were lysed in ACK buffer and washed in Hank's Balanced Salt Solution (HBSS, Thermo Fisher Scientific, 14175-095) containing 2 % FBS. Cells were then incubated with antibodies according to the manufacturer's specifications and analyzed with a BD FACSCelesta™ Flow Cytometer (BD Biosciences). Engraftment and lineage analysis was determined by staining peripheral blood with Mouse monoclonal PE anti-mouse CD45.1, BioLegend, Cat#110708; RRID: AB_313497; Mouse monoclonal FITC anti-mouse CD45.2, BioLegend, Cat#109806; RRID: AB_313443; Rat monoclonal BV421 anti-mouse Ly-6G and Ly-6C, BD Biosciences, Cat#562709; RRID: AB_2737736; Rat monoclonal BV421 anti-mouse CD11b, BD Biosciences, Cat#562605; RRID: AB_11152949; Rat monoclonal BV421 anti-mouse CD45R/B220, BD Biosciences, Cat#562922; RRID: AB_2737894; Hamster monoclonal BV421 anti-mouse CD3e, BD Biosciences, Cat#562600; RRID: AB_11153670. The reconstitution potential of HSCs was further tested by performing secondary and tertiary transplants with 10^6 BM obtained from primary or secondary recipients, respectively, 100 days after their reconstitution.

HSC fitness (donor contribution) was calculated by determining the fraction of $CD45.2^+$ cells in total white blood cells (sum of $CD45.2^+$ and $CD45.1^+$ cells). Statistical significance was calculated using the values of the last time point of the reconstitution. Reconstitution kinetics were assessed by calculating the slope of the degree of donor contribution to the recipient's blood over time (linear regression). We calculated the

slope using the first time-point and the last time point before the degree of donor contribution plateaued. The percentage of myeloid and lymphoid cells was determined by quantifying the fraction of Gr-1$^+$, CD11b$^+$, B220$^+$ or CD3e$^+$ cells that were also CD45.2$^+$. Each lineage marker fraction was normalized to a sum of 100 %.

Homing assays were performed as reconstitution experiments, except 6,000-8,000 donor HSCs were injected. The percentages of donor HSCs in the bone in relation to recipient BM-cells were determined 21 hours after reconstitution.

RNA isolation

For RNA isolation, 10,000 XS, M, XL or not size sorted HSCs in $G_{0/1}$ were isolated as described above but in the absence of FBS. HSCs were sorted into 750 µL TrizolLS. During the sort, the collection sample was vortexed every 10 min. Post-sort, the samples were brought to a total volume of 1 mL with DEPC treated water. Samples were stored at -80 °C or directly used for RNA extraction. To extract RNA, 200 µL chloroform was added to the sample and briefly vortexed at medium speed. After 2 min at RT, the sample was centrifuged at 12,000 x g for 15 min at 4 °C. 400 µL of the aqueous phase was removed and put into 1,400 µL RLT buffer (Qiagen) with 14 µL β-mercaptoethanol and mixed vigorously. 1 mL 100 % ethanol was added to each sample, mixed by pipetting, then loaded onto RNeasy Micro Kit (Qiagen) columns. The manufacturer's directions were followed from the RW1 wash step and the sample was eluted into 14 µL DEPC water.

For RNA-seq analysis, samples were analyzed for RNA integrity using a Femto Analyzer. Then the Clontech v4 Low-Input RNA Kit was used for the PolyA library prep. RNA-seq data were aligned to the mm10 mouse genome assembly and the ensemble version 88 annotation with STAR version 2.5.3a and gene expression was summarized with RSEM version 1.3.0 (*71*).

RNA-seq analysis

The RNA-Seq data is available from the Gene Expression Omnibus under accession number GSE154335. Expression data were analyzed using 2 different data sets: (i) All human GO gene sets msigDb version 7.1 (*84*) and (ii) mouse gene categories of HSCs based on previous studies (*33-40*) (**Table S2**).

Differential expression analysis was performed with R version 3.4.4 and DESeq2 version 1.16.1 (*85*). Differentially expressed genes were defined as those having an absolute log2 fold change greater than 1 and a false discovery rate (FDR) - adjusted p-value of less than 0.05 (*q*-value). Deseq2 and edgeR version 3.4.4 programs were used to perform principle component analysis. Data parsing and clustering was performed using Tibco Spotfire Analyst 7.6.1. Mouse genes were mapped to human orthologs using Pre-ranked. GSEA analysis was performed using javaGSEA version 2.3.0. Differential expression analysis was done by making comparisons between two biological replicates of L, M, and S cell sizes and un-fractioned pool of cells. Very few genes meet the differential expression thresholds of log2 fold change greater than 1 or less than -1 and an adjusted *p*-value less than 0.05 (**Table S3**). Pre-ranked GSEA (version 4.0.3) was run using the DESeq2 Wald statistic as ranking metric and human gene symbols with the MSigDB (https://www.gsea-msigdb.org/gsea/msigdb/index.jsp) of the C5 GO gene sets. Similar runs were performed with mouse gene symbols and a collection of manually curated mouse gene sets. The small number of differentially expressed genes in these comparisons limits the utility of these tools but the data

produced are consistent with the GSEA results. To calculate the percentage of GO gene sets associated with a biological pathway that passed the filter of being different when comparing XS- or M-sized HSCs with XL-HSCs but not different when comparing XS with M-sized HSCs, we determined the total number of GO gene sets associated with the biological process and computed the percentage (**Table S1**).

***In vitro* cultivation of murine and human HSCs**

Flow cytometer-sorted murine or human HSCs were resuspended in 4 mL complete MethoCult GF M3434 medium or MethoCult™ H4435 Enriched (STEMCELL Technologies) thawed at RT and 1 mL of the suspension was placed into 35 mm dishes in triplicates. Growth at 37°C in a 5 % CO_2 chamber was monitored until colonies were visible (7d and 21d, respectively). Number of colonies and colony type were quantified manually.

Protein synthesis assay

Protein synthesis was measured as described in detail before (*47*). In brief: Mice were administered a single dose of OP-Puro (50mg/kg body mass, i.p.) and sacrificed 1 h later. An azidealkyne reaction was used to fluorescently label OP-Puro. Fluorescence intensity (protein synthesis) and cell size (forward scatter) was measured during cytometric analysis.

Measurements of single-cell density and volume using a suspended micro-channel resonator

HSCs were isolated as detailed above and cultured *ex vivo* for 2 days in expansion medium (StemSpan SFEM#09600 supplemented with cytokines). Single-cell density and volume measurements were carried out using the suspended micro-channel resonator (SMR), as detailed previously (*72, 73*). Briefly, the SMR is a vibrating cantilever that has a fluidics micro-channel passing through it. As a cell is flown through the channel in the cantilever, the vibration frequency changes proportionally to the buoyant mass of the cell. The vibration of the cantilever is monitored using piezoresistors. On the other side of the cantilever, the cell is mixed into a denser fluid, in which the cell is flown back through the cantilever to obtain another measurement of the buoyant mass. As the density of the two fluids is known, the absolute volume and density of the cell can be calculated from the two buoyant mass measurements (*73*). This is then followed by flushing another cell into the system for a measurement. The HSC population was continuously sampled this way for 5h. The average density or volume of the cells did not change during the experiment. The two media, in which the cells were measured were expansion medium and expansion medium supplemented with 30% OptiPrep (Sigma-Aldrich). The SMR was maintained at RT throughout the measurements, while the sample of suspended stem cells were kept on ice. The stem cells were mixed by gentle pipetting approximately every 1h in order to avoid cell clumping. Cell doublets were removed during the data analysis using the node deviation signal of the SMR, which differentiates doublets from singlets (*86*). The geometry, physical dimensions, operation of the SMR and data analysis were identical to those reported in (*72*).

Intestinal crypt isolation and organoid formation assay of ISCs

As previously reported (*74*) and briefly summarized here, small intestines were removed from animals, washed with cold PBS, opened longitudinally and then incubated on ice with PBS containing EDTA (10 mM) for 45 min. Tissues were then moved to PBS. Crypts were mechanically separated from the connective

tissue by shaking or by scraping, and then filtered through a 70 µm mesh into a 50 mL conical tube to remove villus material and tissue fragments. Crypts were dissociated into single cells by trypsinization and sorted by flow-cytometry into crypt culture medium, a modified form of medium as described previously (*74*). Isolated ISCs and Paneth cells were then mixed (1:1 ratio, 2,000 cells each), centrifuged, resuspended in 5 µL crypt culture medium and then seeded onto MatrigelTM (Corning 356231 growth factor reduced) containing 1 µM JAG- 1 protein (AnaSpec, AS-61298) in a flat bottom 48-well plate (Corning 3548). The MatrigelTM and cells were allowed to solidify before adding 300 µL of crypt culture medium. Organoid-forming capacity of the sorted ISCs was quantified after 3-5 days of culture. Each frequency was quantified by n > 100 cells per each view and n = 3 views per sample. In average, each frequency was determined from 20 - 30 organoids/ 100 - 300 ISCs.

Drug and irradiation treatments

PD (Palbociclib, PD-0332991, LC Laboratories; 30.4 mg/kg body weight) (*87*), rapamycin (LC Laboratories; 6.4 mg/kg body weight) (*88*) or vehicle was intraperitoneally injected at a volume of 100 µL every 48 h for the indicated treatment time. Average body weight of the mouse was estimated to be 25 g. Rapamycin was reconstituted in ethanol and PD in DMSO. Drugs were then diluted in 20 % DMSO, 40 % PEG 400 (JT Baker) in PBS. Blood composition of treated animals was analyzed after 70 days of treatment. Hematocrit in the peripheral blood was determined. Due to the decline in the Body Condition Score of recipient mice (CD45.1) that received rapamycin treatment after reconstitutions, we reduced the dose frequency to every 72 h. Mice were treated from week 8 with rapamycin (6.4 mg/kg body weight) every 3 days until week 102. Animals were sub-lethally irradiated using a 3, 5 or 6 Gy dosing. HSCs were isolated 14 days after irradiation for cell size analysis, senescence assays and reconstitution assays. The Cre-recombinase was activated via tamoxifen i.p. injections of 2 mg/100 µL per dose. Injections were performed using a 26 G needle (BD Tuberculin Syringes, 309625).

Fluorescence assays

For immunofluorescence analyses, Fisherbrand™ Superfrost™ Plus Microscope Slides were primed with 0.1 % polylysine for 5 min, washed with dH_2O and air-dried. 15,000 sorted HSCs were distributed on slides and incubated for 1 h in a humidified chamber at RT. HSCs were fixed for 20 min at RT with freshly prepared 4% paraformaldehyde (PFA, pH 7.2) and then washed three times with PBS. HSCs were permeabilized for 20 min in 0.2 % Triton-X 100, washed three times with PBS, and blocked for 30 min using 10 % Donkey Serum (Sigma) in PBS. Cells were incubated with primary antibody in 10 % Donkey Serum in PBS overnight at 4 °C: Phospho-S6 Ribosomal Protein (Ser240/244) Rabbit mAb (Cell Signaling Technology, Cat# 5364; RRID:AB_10694233), anti-P-Ser139 γH2XA (Cell Signaling Technology, Cat# 2577; RRID: AB_2118010, 1:100) or anti-Drp1 (Abcam, Cat# ab56788, RRID:AB_941306, 1:100). After HSCs were washed three times with PBS + 0.1 % Tween-20, the secondary antibody solution (1:500, goat anti-rabbit Alexa 488, Cell Signaling Technology, 4412S, 1:500 goat anti-mouse Alexa 488, Invitrogen, A-10680) was added for 1 h at RT in the dark in 10 % Donkey Serum in PBS. Coverslips were mounted with ProLong Gold Antifade Reagent with (Invitrogen, Molecular Probes) and imaged after 12 h. Control slides were not treated with primary antibody. Images were acquired using a DeltaVision Elite microscope (Applied Precision) platform (GE Healthcare Bio-Sciences) equipped with a CoolSNAP HQ2 camera (Roper), 250W Xenon lamps, SoftWoRx software (Applied Precision). Deconvolution was performed using SoftWoRx

software with default settings. Fluorescence quantification and cell diameter measurements were performed with the Fiji software package. Maximum intensity projections of 20 stacks with step size 0.7 µm images were analyzed with ImageJ. For fluorescence mean intensity measurement, a Region Of Interest (ROI) was drawn around the area of interest and the mean intensity was quantified. An identically sized ROI was put next to the area of interest to determine the background mean intensity. Background mean intensity was subtracted from the area of interest mean intensity to yield the mean intensity (AU). Cells that were 2.5 times larger than the mean were excluded from the analysis. When the distribution of mean intensity was similar between independent experiments, but the average mean intensity was different due to microscopy settings, the mean intensity of independent experiments was normalized among each other to the control sample. The nucleus:cytoplasmic ratio was calculated like this: N/C = nucleus area/(cell area - nucleus area).

To detect mitochondrial mass and ROS in HSCs, lineage-depleted BM cells were incubated at 37°C for 15 min with 50 nM of MitoTracker Green (*75, 76*) or 10 µM CM-H_2DCFDA after the staining of HSC surface marker. To create a positive control for ROS, the BM was treated with 20 µM CCCP. The negative control was left unstained. Cells were analyzed using flow cytometry.

To detect senescent HSCs, we used C_{12}FDG (#7188, Setareh Biotech) to measure the activity of the senescence biomarker SA-β-galactosidase in un-fixed HSCs by flow cytometry (*77*). For fluorescence detection of SA-β-galactosidase activity, 10^7 BM cell/mL were incubated with 30 µM chloroquine (#C6628-25G, Sigma Aldrich) in IMDM supplemented with 2 % FBS at 37°C for 30 min. 32 µM C_{12}-FDG, a β-galactosidase substrate that generates a fluorescent product upon cleavage, was added for 30 min in a 37°C water bath. Cells were washed with 2 % IMDM at 4°C, lineage positive cells were depleted, lin-negative cells stained with HSC antibodies as described above and analyzed by flow cytometry. Unchanged forward and side scatter measures of cells was asserted after dye-treatment. The gates for senescent cells were set based on unstained HSCs controls.

Intensity of the HSC cell surface markers CD48, Slamf1/CD150, cKit, Ly6a/Sca1 and CD34 was quantified using flow cytometry and represented as surface concentration (fluorescence intensity (AU)/µm^2) using the cell surface area determined using a Coulter Counter.

Imaging and quantification of fibrillarin-stained nucleolus

Immuno-fluorescent images were acquired using a laser-scanning confocal microscope (Leica TCS SP8-X) using the Lightning mode with a 100× oil immersion/1.46 NA objective using a 1.28 optical zoom. Leica Applications Suite X 3.5.5.19976 software was used for image acquisition. Images of 2328×2328 pixels were obtained using zoom factor 1.28, resulting in a pixel size of 39.18 ×339.18 nm and pixel dwell time of 344 nm. For imaging DAPI, a 405 nm UV laser line was used (10% intensity) and emission was collected at 441-479 nm using a hybrid detector. An argon laser was used for detection Alexa Fluor 488 (excitation 488 nm; 30% laser power; 2% intensity) and emission was collected at 510-531 nm using a hybrid detector. Sequential scanning was used to prevent crosstalk between the DAPI and the AlexaFluor 488 detection and gain was adjusted to prevent pixel saturation. A minimum of 300 cells was imaged using the Mark and Find module. Z-stacks were set individually for each location using a z-step size of 0.2.

The area of the nucleolus (marked by fibrillarin-AlexaFluor 488) and the area of the nucleus (marked by DAPI and acting as a proxy for cell size) were measured in Fiji (ImageJ 1.52p) for analysis. Each channel was subjected to Z-projection using the "standard deviation" method and converted to binary using default settings. Regions of interest (ROIs) were defined as being individual nucleoli in the fibrillarin-AlexaFluor 488 channel and as individual nuclei in the DAPI channel. The ROIs were measured and the overall nucleolar area (defined as the sum area of all nucleoli in the cell), as well as the number of nucleoli were related to nuclear size, which correlates to cell size (data not shown). The nuclear areas were grouped into three categories: XS (which included the smallest 10% of nuclei), M (which included the mean 20% of nuclei by size) and XL (which covered the largest 10% of nuclei).

Comet Assay

DNA damage in freshly collected HSCs was assessed performing a Comet Assay. 15,000 HSCs were collected per sample.

CometChip fabrication and cell loading: The CometChip PDMS molds were fabricated using the protocols described by (*75*). 1% UltraPure™ agarose (16500 Invitrogen) was dissolved in PBS and poured on top of a sheet of GelBond film (53761 Lonza). A mold with 25 µm diameter microposts was placed on the 1% UltraPure™ agarose. After 5 minutes, the mold was removed, leaving the agarose gel with microwells attached to the Gelbond film. The film was placed on a glass plate before being fixed between the plate and a bottomless 96-well plate (655000 Greiner BioOne). Once the gel was clamped in place, 50 µL of the HSC solution were pipetted into each of the 96-wells and captured in microwells by gravity. The gel was rinsed with PBS then covered with 1% UltraPure™ Low Melting Point Agarose (16520050 Thermo Fisher Scientific).

FPG Treatment and CometChip Assay: The CometChip gel was incubated overnight at 4 °C in freshly made alkaline lysis stock (2.5 M NaCl, 100 mM Na_2EDTA, 10 mM Tris, 1 % Triton X-100) to allow for DNA unwinding. After overnight lysis, the CometChip was washed three times with PBS before being incubated for 1 h at RT in FPG (M0240S New England Biolabs) diluted $1{:}10^4$ in PBS. The CometChip was then incubated at 4 °C in alkaline electrophoresis buffer (0.3 M NaOH, 1 mM Na_2EDTA) for 40 min at 4 °C. Next, electrophoresis was performed at 4 °C in the alkaline electrophoresis buffer at 1 V/cm and a current of 300 mA. The CometChip was neutralized by two 15-min washes in neutralization buffer (0.4 M Tris-HCl at pH 7.5) at RT.

Fluorescence and CometChip Analysis: Following neutralization, the CometChip was stained with SYBR Gold (S11494Invitrogen) at a concentration of $1{:}10^4$ diluted in PBS. Images were captured with the 4 x objective of a Nikon 80i upright microscope and analyzed using the Guicometanalyzer, a custom software written in MatLab (The Mathworks) (*78*).

Metabolite measurements in HSCs using liquid chromatography-mass spectrometry (LC-MS)

Water Soluble Metabolites: Methods for the isolation of cells for metabolomics were previously described (*79*). Here in brief, during the isolation, cells were kept cold. FACSAria flow cytometer was washed with ethanol and Milli-Q deionized water before the experiment and HSCs were sorted with a sheath fluid of 0.5× PBS, prepared fresh using Milli-Q water (Millipore), and a 70-µm nozzle in a four-way purity sort mode. 10,000 HSCs were directly sorted into 150 uL acetonnitril:methanol:water (40:40:20) pre-chilled low-binding eppendorf tubes and maintained at 4 °C during sorting. No FBS was used during the

procedure. Samples that were sorted for no cells were used as a control. After sorting, each sample was kept on dry ice for the duration of the experiment, and then stored at −80 °C. The supernatants were centrifuged at 16,000 x g for 20 min to remove any residual debris before analysis.

The LC-MS method involved hydrophilic interaction chromatography (HILIC) coupled to the Q Exactive PLUS mass spectrometer (Thermo Scientific). The LC separation was performed on a XBridge BEH Amide column (150 mm 3 2.1 mm, 2.5 mm particle size, Waters, Milford, MA). Solvent A is 95%: 5% H2O: acetonitrile with 20 mM ammonium bicarbonate, and solvent B is acetonitrile. The gradient was 0 min, 85% B; 2 min, 85% B; 3 min, 80% B; 5 min, 80% B; 6 min, 75% B; 7 min, 75% B; 8 min, 70% B; 9 min, 70% B; 10 min, 50% B; 12 min, 50% B; 13 min, 25% B; 16 min, 25% B; 18 min, 0% B; 23 min, 0% B; 24 min, 85% B; 30 min, 85% B. Other LC parameters: flow rate 150 ml/min, column temperature 25°C, injection volume 10 μL and autosampler temperature was 5°C. The mass spectrometer was operated in both negative and positive ion mode for the detection of metabolites (*89*). Other MS parameters: resolution of 140,000 at m/z 200, automatic gain control (AGC) target at 3e6, maximum injection time of 30 ms and scan range of m/z 75-1000. Raw LC-MS data were converted to mzXML format using the command line "msconvert" utility (*90*). Data were analyzed via the El-Maven software (*91*).

Quantification, statistical analysis, data availability

Guidelines for quantification, statistical analysis, data availability have been followed. Each experiment was repeated with three mice or as indicated (biological replicates). Representative experiments are shown only if the experiment was repeated three times and the results of each one supported the same conclusion. Standard deviations (SD) of the mean of three independent data points are shown in graphs or as indicated. Asterisks indicate P values: ****P < 0.0001, ***P < 0.001, **P < 0.01, *P < 0.05; NS, not significant. For all panels, statistical significance was calculated using unpaired *t*-test to compare two samples, One Way Analysis Of Variance (ANOVA)- multiple comparison - Tukey post-hoc test to compare multiple (three or more) samples or otherwise specified. Values were only excluded if most extreme value in the data set was a significant outlier from the rest (P < 0.05) according to Grubbs' test. No statistical method was used to predetermine sample size.

REFERENCES AND NOTES

1. R. Yamamoto, A. C. Wilkinson, J. Ooehara, X. Lan, C. Y. Lai, Y. Nakauchi, J. K. Pritchard, H. Nakauchi, Large-scale clonal analysis resolves aging of the mouse hematopoietic stem cell compartment. *Cell Stem Cell* **22**, 600–607.e4 (2018).

2. R. A. Saxton, D. M. Sabatini, mTOR signaling in growth, metabolism, and disease. *Cell* **168**, 960–976 (2017).

3. E. M. Pietras, M. R. Warr, E. Passegue, Cell cycle regulation in hematopoietic stem cells. *J. Cell Biol.* **195**, 709–720 (2011).

4. L. M. Kamminga, R. van Os, A. Ausema, E. J. Noach, E. Weersing, B. Dontje, E. Vellenga, G. de Haan, Impaired hematopoietic stem cell functioning after serial transplantation and during normal aging. *Stem Cells* **23**, 82–92 (2005).

5. J. Campisi, Aging, cellular senescence, and cancer. *Annu. Rev. Physiol.* **75**, 685–705 (2013).

6. C. E. Burd, J. A. Sorrentino, K. S. Clark, D. B. Darr, J. Krishnamurthy, A. M. Deal, N. Bardeesy, D. H. Castrillon, D. H. Beach, N. E. Sharpless, Monitoring tumorigenesis and senescence in vivo with a p16(INK4a)-luciferase model. *Cell* **152**, 340–351 (2013).

7. A. Biran, L. Zada, P. Abou Karam, E. Vadai, L. Roitman, Y. Ovadya, Z. Porat, V. Krizhanovsky, Quantitative identification of senescent cells in aging and disease. *Aging Cell* **16**, 661–671 (2017).

8. U. Herbig, M. Ferreira, L. Condel, D. Carey, J. M. Sedivy, Cellular senescence in aging primates. *Science* **311**, 1257 (2006).

9. Y. Mitsui, E. L. Schneider, Relationship between cell replication and volume in senescent human diploid fibroblasts. *Mech. Ageing Dev.* **5**, 45–56 (1976).

10. L. Hayflick, P. S. Moorhead, The serial cultivation of human diploid cell strains. *Exp. Cell Res.* **25**, 585–621 (1961).

11. D. C. Fingar, S. Salama, C. Tsou, E. Harlow, J. Blenis, Mammalian cell size is controlled by mTOR and its downstream targets S6K1 and 4EBP1/eIF4E. *Genes Dev.* **16**, 1472–1487 (2002).

12. G. E. Neurohr, R. L. Terry, J. Lengefeld, M. Bonney, G. P. Brittingham, F. Moretto, T. P. Miettinen, L. P. Vaites, L. M. Soares, J. A. Paulo, J. W. Harper, S. Buratowski, S. Manalis, F. J. van Werven, L. J. Holt, A. Amon, Excessive cell growth causes cytoplasm dilution and contributes to senescence. *Cell* **176**, 1083–1097.e18 (2019).

13. R. K. Mortimer, J. R. Johnston, Life span of individual yeast cells. *Nature* **183**, 1751–1752 (1959).

14. P. M. Bemiller, J. E. Miller, Cytological changes senescing WI-38 cells: A statistical analysis. *Mech. Ageing Dev.* **10**, 1–15 (1979).

15. A. Denoth Lippuner, T. Julou, Y. Barral, Budding yeast as a model organism to study the effects of age. *FEMS Microbiol. Rev.* **38**, 300–325 (2014).

16. Z. N. Demidenko, M. V. Blagosklonny, Growth stimulation leads to cellular senescence when the cell cycle is blocked. *Cell Cycle* **7**, 3355–3361 (2008).

17. L. Shao, W. Feng, H. Li, D. Gardner, Y. Luo, Y. Wang, L. Liu, A. Meng, N. E. Sharpless, D. Zhou, Total body irradiation causes long-term mouse BM injury via induction of HSC premature senescence in an Ink4a- and Arf-independent manner. *Blood* **123**, 3105–3115 (2014).

18. B. M. Moehrle, K. Nattamai, A. Brown, M. C. Florian, M. Ryan, M. Vogel, C. Bliederhaeuser, K. Soller, D. R. Prows, A. Abdollahi, D. Schleimer, D. Walter, M. D. Milsom, P. Stambrook, M. Porteus, H. Geiger, Stem cell-specific mechanisms ensure genomic fidelity within HSCs and upon aging of HSCs. *Cell Rep.* **13**, 2412–2424 (2015).

19. S. He, P. J. Roberts, J. A. Sorrentino, J. E. Bisi, H. Storrie-White, R. G. Tiessen, K. M. Makhuli, W. A. Wargin, H. Tadema, E. J. van Hoogdalem, J. C. Strum, R. Malik, N. E. Sharpless, Transient CDK4/6 inhibition protects hematopoietic stem cells from chemotherapy-induced exhaustion. *Sci. Transl. Med.* **9**, eaal3986 (2017).

20. J. M. Bernitz, H. S. Kim, B. MacArthur, H. Sieburg, K. Moore, Hematopoietic stem cells count and remember self-renewal divisions. *Cell* **167**, 1296–1309.10 (2016).

21. S. J. Morrison, I. L. Weissman, The long-term repopulating subset of hematopoietic stem cells is deterministic and isolatable by phenotype. *Immunity* **1**, 661–673 (1994).

22. T. P. Miettinen, M. Bjorklund, Cellular allometry of mitochondrial functionality establishes the optimal cell size. *Dev. Cell* **39**, 370–382 (2016).

23. B. Gan, E. Sahin, S. Jiang, A. Sanchez-Aguilera, K. L. Scott, L. Chin, D. A. Williams, D. J. Kwiatkowski, R. A. DePinho, mTORC1-dependent and -independent regulation of stem cell renewal, differentiation, and mobilization. *Proc. Natl. Acad. Sci. U.S.A.* **105**, 19384–19389 (2008).

24. A. Wilson, E. Laurenti, G. Oser, R. C. van der Wath, W. Blanco-Bose, M. Jaworski, S. Offner, C. F. Dunant, L. Eshkind, E. Bockamp, P. Lio, H. R. Macdonald, A. Trumpp, Hematopoietic stem cells reversibly switch from dormancy to self-renewal during homeostasis and repair. *Cell* **135**, 1118–1129 (2008).

25. D. Nakada, H. Oguro, B. P. Levi, N. Ryan, A. Kitano, Y. Saitoh, M. Takeichi, G. R. Wendt, S. J. Morrison, Oestrogen increases haematopoietic stem-cell self-renewal in females and during pregnancy. *Nature* **505**, 555–558 (2014).

26. E. Passegue, A. J. Wagers, S. Giuriato, W. C. Anderson, I. L. Weissman, Global analysis of proliferation and cell cycle gene expression in the regulation of hematopoietic stem and progenitor cell fates. *J. Exp. Med.* **202**, 1599–1611 (2005).

27. A. Foudi, K. Hochedlinger, D. Van Buren, J. W. Schindler, R. Jaenisch, V. Carey, H. Hock, Analysis of histone 2B-GFP retention reveals slowly cycling hematopoietic stem cells. *Nat. Biotechnol.* **27**, 84–90 (2009).

28. J. Flach, S. T. Bakker, M. Mohrin, P. C. Conroy, E. M. Pietras, D. Reynaud, S. Alvarez, M. E. Diolaiti, F. Ugarte, E. C. Forsberg, M. M. Le Beau, B. A. Stohr, J. Mendez, C. G. Morrison, E. Passegue, Replication stress is a potent driver of functional decline in ageing haematopoietic stem cells. *Nature* **512**, 198–202 (2014).

29. D. Walter, A. Lier, A. Geiselhart, F. B. Thalheimer, S. Huntscha, M. C. Sobotta, B. Moehrle, D. Brocks, I. Bayindir, P. Kaschutnig, K. Muedder, C. Klein, A. Jauch, T. Schroeder, H. Geiger, T. P. Dick, T. Holland-Letz, P. Schmezer, S. W. Lane, M. A. Rieger, M. A. Essers, D. A. Williams, A. Trumpp, M. D. Milsom, Exit from dormancy provokes DNA-damage-induced attrition in haematopoietic stem cells. *Nature* **520**, 549–552 (2015).

30. T. Sperka, J. Wang, K. L. Rudolph, DNA damage checkpoints in stem cells, ageing and cancer. *Nat. Rev. Mol. Cell Biol.* **13**, 579–590 (2012).

31. S. J. Pfau, R. E. Silberman, K. A. Knouse, A. Amon, Aneuploidy impairs hematopoietic stem cell fitness and is selected against in regenerating tissues in vivo. *Genes Dev.* **30**, 1395–1408 (2016).

32. W. H. Fleming, E. J. Alpern, N. Uchida, K. Ikuta, G. J. Spangrude, I. L. Weissman, Functional heterogeneity is associated with the cell cycle status of murine hematopoietic stem cells. *J. Cell Biol.* **122**, 897–902 (1993).

33. S. M. Chambers, N. C. Boles, K. Y. Lin, M. P. Tierney, T. V. Bowman, S. B. Bradfute, A. J. Chen, A. A. Merchant, O. Sirin, D. C. Weksberg, M. G. Merchant, C. J. Fisk, C. A. Shaw, M. A. Goodell, Hematopoietic fingerprints: An expression database of stem cells and their progeny. *Cell Stem Cell* **1**, 578–591 (2007).

34. C. Montrone, K. D. Kokkaliaris, D. Loeffler, M. Lechner, G. Kastenmuller, T. Schroeder, A. Ruepp, HSC-explorer: A curated database for hematopoietic stem cells. *PLOS ONE* **8**, e70348 (2013).

35. E. Montecino-Rodriguez, Y. Kong, D. Casero, A. Rouault, K. Dorshkind, P. D. Pioli, Lymphoid-biased hematopoietic stem cells are maintained with age and efficiently generate lymphoid progeny. *Stem Cell Rep.* **12**, 584–596 (2019).

36. J. Yang, Y. Tanaka, M. Seay, Z. Li, J. Jin, L. X. Garmire, X. Zhu, A. Taylor, W. Li, G. Euskirchen, S. Halene, Y. Kluger, M. P. Snyder, I. H. Park, X. Pan, S. M. Weissman, Single cell transcriptomics reveals unanticipated features of early hematopoietic precursors. *Nucleic Acids Res.* **45**, 1281–1296 (2017).

37. N. Cabezas-Wallscheid, D. Klimmeck, J. Hansson, D. B. Lipka, A. Reyes, Q. Wang, D. Weichenhan, A. Lier, L. von Paleske, S. Renders, P. Wünsche, P. Zeisberger, D. Brocks, L. Gu, C. Herrmann, S. Haas, M. A. G. Essers, B. Brors, R. Eils, W. Huber, M. D. Milsom, C. Plass, J. Krijgsveld, A. Trumpp, Identification of regulatory networks in HSCs and their immediate progeny via integrated proteome, transcriptome, and DNA methylome analysis. *Cell Stem Cell* **15**, 507–522 (2014).

38. M. Mann, A. Mehta, C. G. de Boer, M. S. Kowalczyk, K. Lee, P. Haldeman, N. Rogel, A. R. Knecht, D. Farouq, A. Regev, D. Baltimore, Heterogeneous responses of hematopoietic stem cells to inflammatory stimuli are altered with age. *Cell Rep.* **25**, 2992–3005 e5 (2018).

39. E. M. Pietras, D. Reynaud, Y. A. Kang, D. Carlin, F. J. Calero-Nieto, A. D. Leavitt, J. M. Stuart, B. Göttgens, E. Passegué, Functionally distinct subsets of lineage-biased multipotent progenitors control blood production in normal and regenerative conditions. *Cell Stem Cell* **17**, 35–46 (2015).

40. N. K. Wilson, D. G. Kent, F. Buettner, M. Shehata, I. C. Macaulay, F. J. Calero-Nieto, M. Sánchez Castillo, C. A. Oedekoven, E. Diamanti, R. Schulte, C. P. Ponting, T. Voet, C. Caldas, J. Stingl, A. R. Green, F. J. Theis, B. Göttgens, Combined single-cell functional and gene expression analysis resolves heterogeneity within stem cell populations. *Cell Stem Cell* **16**, 712–724 (2015).

41. J. T. Rodgers, K. Y. King, J. O. Brett, M. J. Cromie, G. W. Charville, K. K. Maguire, C. Brunson, N. Mastey, L. Liu, C. R. Tsai, M. A. Goodell, T. A. Rando, mTORC1 controls the adaptive transition of quiescent stem cells from G0 to G(Alert). *Nature* **510**, 393–396 (2014).

42. T. T. Ho, M. R. Warr, E. R. Adelman, O. M. Lansinger, J. Flach, E. V. Verovskaya, M. E. Figueroa, E. Passegue, Autophagy maintains the metabolism and function of young and old stem cells. *Nature* **543**, 205–210 (2017).

43. A. Hinge, J. He, J. Bartram, J. Javier, J. Xu, E. Fjellman, H. Sesaki, T. Li, J. Yu, M. Wunderlich, J. Mulloy, M. Kofron, N. Salomonis, H. L. Grimes, M. D. Filippi, Asymmetrically segregated mitochondria provide cellular memory of hematopoietic stem cell replicative history and drive HSC attrition. *Cell Stem Cell* **26**, 420–430.e6 (2020).

44. M. Delarue, G. P. Brittingham, S. Pfeffer, I. V. Surovtsev, S. Pinglay, K. J. Kennedy, M. Schaffer, J. I. Gutierrez, D. Sang, G. Poterewicz, J. K. Chung, J. M. Plitzko, J. T. Groves, C. Jacobs-Wagner, B. D. Engel, L. J. Holt, mTORC1 controls phase separation and the biophysical properties of the cytoplasm by tuning crowding. *Cell* **174**, 338–349.e20 (2018).

45. C. Mayer, I. Grummt, Ribosome biogenesis and cell growth: mTOR coordinates transcription by all three classes of nuclear RNA polymerases. *Oncogene* **25**, 6384–6391 (2006).

46. V. Tiku, A. Antebi, Nucleolar function in lifespan regulation. *Trends Cell Biol.* **28**, 662–672 (2018).

47. L. Hidalgo San Jose, R. A. J. Signer, Cell-type-specific quantification of protein synthesis in vivo. *Nat. Protoc.* **14**, 441–460 (2019).

48. E. Zatulovskiy, S. Zhang, D. F. Berenson, B. R. Topacio, J. M. Skotheim, Cell growth dilutes the cell cycle inhibitor Rb to trigger cell division. *Science* **369**, 466–471 (2020).

49. D. Daria, M. D. Filippi, E. S. Knudsen, R. Faccio, Z. Li, T. Kalfa, H. Geiger, The retinoblastoma tumor suppressor is a critical intrinsic regulator for hematopoietic stem and progenitor cells under stress. *Blood* **111**, 1894–1902 (2008).

50. C. R. Walkley, S. H. Orkin, Rb is dispensable for self-renewal and multilineage differentiation of adult hematopoietic stem cells. *Proc. Natl. Acad. Sci. U.S.A.* **103**, 9057–9062 (2006).

51. B. E. Keyes, E. Fuchs, Stem cells: Aging and transcriptional fingerprints. *J. Cell Biol.* **217**, 79–92 (2018).

52. V. Tiku, C. Jain, Y. Raz, S. Nakamura, B. Heestand, W. Liu, M. Spath, H. E. D. Suchiman, R. U. Muller, P. E. Slagboom, L. Partridge, A. Antebi, Small nucleoli are a cellular hallmark of longevity. *Nat. Commun.* **8**, 16083 (2017).

53. K. Kirschner, T. Chandra, V. Kiselev, D. Flores-Santa Cruz, I. C. Macaulay, H. J. Park, J. Li, D. G. Kent, R. Kumar, D. C. Pask, T. L. Hamilton, M. Hemberg, W. Reik, A. R. Green, Proliferation drives aging-related functional decline in a subpopulation of the hematopoietic stem cell compartment. *Cell Rep.* **19**, 1503–1511 (2017).

54. D. C. Colter, I. Sekiya, D. J. Prockop, Identification of a subpopulation of rapidly self-renewing and multipotential adult stem cells in colonies of human marrow stromal cells. *Proc. Natl. Acad. Sci. U.S.A.* **98**, 7841–7845 (2001).

55. I. Virant-Klun, M. Stimpfel, Novel population of small tumour-initiating stem cells in the ovaries of women with borderline ovarian cancer. *Sci. Rep.* **6**, 34730 (2016).

56. H. E. Young, C. Duplaa, M. J. Yost, N. L. Henson, J. A. Floyd, K. Detmer, A. J. Thompson, S. W. Powell, T. C. Gamblin, K. Kizziah, B. J. Holland, A. Boev, J. M. Van De Water, D. C. Godbee, S. Jackson, M. Rimando, C. R. Edwards, E. Wu, C. Cawley, P. D. Edwards, A. Macgregor, R. Bozof, T. M. Thompson, G. J. Petro, H. M. Shelton, B. L. McCampbell, J. C. Mills, F. L. Flynt, T. A. Steele, M. Kearney, A. Kirincich-Greathead, W. Hardy, P. R. Young, A. V. Amin, R. S. Williams, M. M. Horton, S. McGuinn, K. C. Hawkins, K. Ericson, L. Terracio, C. Moreau, D. Hixson, B. W. Tobin, J. Hudson, F. P. Bowyer, A. C. Black Jr., Clonogenic analysis reveals reserve stem cells in postnatal mammals. II. Pluripotent epiblastic-like stem cells. *Anat Rec A Discov Mol Cell Evol Biol* **277**, 178–203 (2004).

57. N. S. Chandel, H. Jasper, T. T. Ho, E. Passegue, Metabolic regulation of stem cell function in tissue homeostasis and organismal ageing. *Nat. Cell Biol.* **18**, 823–832 (2016).

58. S. Xie, J. M. Skotheim, A G1 sizer coordinates growth and division in the mouse epidermis. *Curr. Biol.* **30**, 916–924.e2 (2020).

59. M. B. Ginzberg, R. Kafri, M. Kirschner, Cell biology. On being the right (cell) size. *Science* **348**, 1245075 (2015).

60. M. Bjorklund, Cell size homeostasis: Metabolic control of growth and cell division. *Biochim. Biophys. Acta Mol. Cell Res.* **1866**, 409–417 (2019).

61. M. B. Ginzberg, N. Chang, H. D'Souza, N. Patel, R. Kafri, M. W. Kirschner, Cell size sensing in animal cells coordinates anabolic growth rates and cell cycle progression to maintain cell size uniformity. *eLife* **7**, e26957 (2018).

62. C. Cadart, S. Monnier, J. Grilli, P. J. Saez, N. Srivastava, R. Attia, E. Terriac, B. Baum, M. Cosentino-Lagomarsino, M. Piel, Size control in mammalian cells involves modulation of both growth rate and cell cycle duration. *Nat. Commun.* **9**, 3275 (2018).

63. P. Jorgensen, M. Tyers, How cells coordinate growth and division. *Curr. Biol.* **14**, R1014-R1027 (2004).

64. Y. Chen, G. Zhao, J. Zahumensky, S. Honey, B. Futcher, Differential scaling of gene expression with cell size may explain size control in budding yeast. *Mol. Cell* **78**, 359–370.e6 (2020).

65. J. Yang, H. Dungrawala, H. Hua, A. Manukyan, L. Abraham, W. Lane, H. Mead, J. Wright, B. L. Schneider, Cell size and growth rate are major determinants of replicative lifespan. *Cell Cycle* **10**, 144–155 (2011).

66. R. A. Signer, J. A. Magee, A. Salic, S. J. Morrison, Haematopoietic stem cells require a highly regulated protein synthesis rate. *Nature* **509**, 49–54 (2014).

67. M. Kaeberlein, P. S. Rabinovitch, G. M. Martin, Healthy aging: The ultimate preventative medicine. *Science* **350**, 1191–1193 (2015).

68. S. Mahmoudi, L. Xu, A. Brunet, Turning back time with emerging rejuvenation strategies. *Nat. Cell Biol.* **21**, 32–43 (2019).

69. M. J. Kiel, Ö. H. Yilmaz, T. Iwashita, O. H. Yilmaz, C. Terhorst, S. J. Morrison, SLAM family receptors distinguish hematopoietic stem and progenitor cells and reveal endothelial niches for stem cells. *Cell* **121**, 1109–1121 (2005).

70. F. Notta, S. Doulatov, E. Laurenti, A. Poeppl, I. Jurisica, J. E. Dick, Isolation of single human hematopoietic stem cells capable of long-term multilineage engraftment. *Science* **333**, 218–221 (2011).

71. B. Li, C. N. Dewey, RSEM: Accurate transcript quantification from RNA-Seq data with or without a reference genome. *BMC Bioinformatics* **12**, 323 (2011).

72. S. Son, J. H. Kang, S. Oh, M. W. Kirschner, T. J. Mitchison, S. Manalis, Resonant microchannel volume and mass measurements show that suspended cells swell during mitosis. *J. Cell Biol.* **211**, 757–763 (2015).

73. W. H. Grover, A. K. Bryan, M. Diez-Silva, S. Suresh, J. M. Higgins, S. R. Manalis, Measuring single-cell density. *Proc. Natl. Acad. Sci. U.S.A.* **108**, 10992–10996 (2011).

74. M. M. Mihaylova, C.-W. Cheng, A. Q. Cao, S. Tripathi, M. D. Mana, K. E. Bauer-Rowe, M. Abu-Remaileh, L. Clavain, A. Erdemir, C. A. Lewis, E. Freinkman, A. S. Dickey, A. R. La Spada, Y. Huang, G. W. Bell, V. Deshpande, P. Carmeliet, P. Katajisto, D. M. Sabatini, Ö. H. Yilmaz, Fasting activates fatty acid oxidation to enhance intestinal stem cell function during homeostasis and aging. *Cell Stem Cell* **22**, 769–778.e4 (2018).

75. W. Pendergrass, N. Wolf, M. Poot, Efficacy of MitoTracker Green and CMXrosamine to measure changes in mitochondrial membrane potentials in living cells and tissues. *Cytometry A* **61A**, 162–169 (2004).

76. M. J. de Almeida, L. L. Luchsinger, D. J. Corrigan, L. J. Williams, H. W. Snoeck, Dye-independent methods reveal elevated mitochondrial mass in hematopoietic stem cells. *Cell Stem Cell* **21**, 725–729.e4 (2017).

77. F. Debacq-Chainiaux, J. D. Erusalimsky, J. Campisi, O. Toussaint, Protocols to detect senescence-associated beta-galactosidase (SA-betagal) activity, a biomarker of senescent cells in culture and in vivo. *Nat. Protoc.* **4**, 1798–1806 (2009).

78. D. K. Wood, D. M. Weingeist, S. N. Bhatia, B. P. Engelward, Single cell trapping and DNA damage analysis using microwell arrays. *Proc. Natl. Acad. Sci. U.S.A.* **107**, 10008–10013 (2010).

79. M. Agathocleous, C. E. Meacham, R. J. Burgess, E. Piskounova, Z. Zhao, G. M. Crane, B. L. Cowin, E. Bruner, M. M. Murphy, W. Chen, G. J. Spangrude, Z. Hu, R. J. DeBerardinis, S. J. Morrison, Ascorbate regulates haematopoietic stem cell function and leukaemogenesis. *Nature* **549**, 476–481 (2017).

80. A. Ventura, D. G. Kirsch, M. E. McLaughlin, D. A. Tuveson, J. Grimm, L. Lintault, J. Newman, E. E. Reczek, R. Weissleder, T. Jacks, Restoration of p53 function leads to tumour regression in vivo. *Nature* **445**, 661–665 (2007).

81. D. J. Kwiatkowski, H. Zhang, J. L. Bandura, K. M. Heiberger, M. Glogauer, N. el-Hashemite, H. Onda, A mouse model of TSC1 reveals sex-dependent lethality from liver hemangiomas, and up-regulation of p70S6 kinase activity in Tsc1 null cells. *Hum. Mol. Genet.* **11**, 525–534 (2002).

82. S. Marino, M. Vooijs, H. van Der Gulden, J. Jonkers, A. Berns, Induction of medulloblastomas in p53-null mutant mice by somatic inactivation of Rb in the external granular layer cells of the cerebellum. *Genes Dev.* **14**, 994–1004 (2000).

83. W. W. Pang, E. A. Price, D. Sahoo, I. Beerman, W. J. Maloney, D. J. Rossi, S. L. Schrier, I. L. Weissman, Human bone marrow hematopoietic stem cells are increased in frequency and myeloid-biased with age. *Proc. Natl. Acad. Sci. U.S.A.* **108**, 20012–20017 (2011).

84. A. Subramanian, P. Tamayo, V. K. Mootha, S. Mukherjee, B. L. Ebert, M. A. Gillette, A. Paulovich, S. L. Pomeroy, T. R. Golub, E. S. Lander, J. P. Mesirov, Gene set enrichment analysis: A knowledge-based approach for interpreting genome-wide expression profiles. *Proc. Natl. Acad. Sci. U.S.A.* **102**, 15545–15550 (2005).

85. S. Anders, W. Huber, Differential expression analysis for sequence count data. *Genome Biol.* **11**, R106 (2010).

86. J. H. Kang, T. P. Miettinen, L. Chen, S. Olcum, G. Katsikis, P. S. Doyle, S. R. Manalis, Noninvasive monitoring of single-cell mechanics by acoustic scattering. *Nat. Methods* **16**, 263–269 (2019).

87. I. Z. Uras, G. J. Walter, R. Scheicher, F. Bellutti, M. Prchal-Murphy, A. S. Tigan, P. Valent, F. H. Heidel, S. Kubicek, C. Scholl, S. Fröhling, V. Sexl, Palbociclib treatment of FLT3-ITD+ AML cells uncovers a kinase-dependent transcriptional regulation of FLT3 and PIM1 by CDK6. *Blood* **127**, 2890–2902 (2016).

88. C. Chen, Y. Liu, Y. Liu, P. Zheng, mTOR regulation and therapeutic rejuvenation of aging hematopoietic stem cells. *Sci. Signal.* **2**, ra75 (2009).

89. L. Wang, X. Xing, L. Chen, L. Yang, X. Su, H. Rabitz, W. Lu, J. D. Rabinowitz, Peak annotation and verification engine for untargeted LC-MS metabolomics. *Anal. Chem.* **91**, 1838–1846 (2019).

90. R. Adusumilli, P. Mallick, Data conversion with ProteoWizard msConvert. *Methods Mol. Biol.* **1550**, 339–368 (2017).

91. S. Agrawal, S. Kumar, R. Sehgal, S. George, R. Gupta, S. Poddar, A. Jha, S. Pathak, El-MAVEN: A fast, robust, and user-friendly mass spectrometry data processing engine for metabolomics. *Methods Mol. Biol.* **1978**, 301–321 (2019).